FILE COPY
NO 6

N62 60921

NACA RM L51E07

1035

NACA

RESEARCH MEMORANDUM

SYSTEM ANALYSES AND AUTOPILOT DESIGN FOR AUTOMATIC ROLL STABILIZATION OF A SUPERSONIC PILOTLESS AIRCRAFT

By Jacob Zarovsky

Langley Aeronautical Laboratory
Langley Field, Va.

THIS DOCUMENT ON LOAN FROM THE FILES OF

NATIONAL ADVISORY COMMITTEE FOR AERONAUTICS
LANGLEY AERONAUTICAL LABORATORY
LANGLEY FIELD, HAMPTON, VIRGINIA

RETURN TO THE ABOVE ADDRESS.

REQUESTS FOR PUBLICATIONS SHOULD BE ADDRESSED AS FOLLOWS:

NATIONAL ADVISORY COMMITTEE FOR AERONAUTICS
1512 H STREET, N. W.
WASHINGTON 25, D. C.

NATIONAL ADVISORY COMMITTEE
FOR AERONAUTICS

WASHINGTON

July 11, 1951

NACA RM L51E07

NATIONAL ADVISORY COMMITTEE FOR AERONAUTICS

RESEARCH MEMORANDUM

SYSTEM ANALYSES AND AUTOPILOT DESIGN FOR AUTOMATIC ROLL STABILIZATION OF A SUPERSONIC PILOTLESS AIRCRAFT

By Jacob Zarovsky

SUMMARY

System analyses and autopilot design procedure have been carried out for a supersonic pilotless aircraft with twin jet engines. The autopilots investigated were a gyro-actuated control, a gyro-actuated control with a rate-sensing device (to provide additional damping), and an electronic-hydraulic autopilot. The electronic-hydraulic autopilot with a passive electrical lead network and suitable gain adjustment was found to provide acceptable system characteristics and appears to be a practical means of providing roll stabilization.

The graphical methods employed in the analysis indicate a direct approach to autopilot design.

INTRODUCTION

The maneuvering characteristics of many pilotless aircraft result in stringent roll-stabilization requirements. Flight at simultaneous angles of attack and sideslip may induce large rolling moments due to cross-coupling between pitching and yawing of the aircraft. (See reference 1.)

The factors in supersonic pilotless aircraft design that contribute to efficient structures and desirable lift and drag characteristics, such as low-aspect-ratio wings and swept, tapered, thin wings, generally result in poor roll damping and undesirable roll-control-surface characteristics. The roll autopilot must compensate for the undesirable airframe characteristics if roll stabilization of an airframe is required.

The purpose of this paper is to present the system analysis and the detailed design procedure conducted in connection with roll position stabilization of a supersonic pilotless aircraft with twin jet engines. A sketch of this airframe is shown in figure 1. The wing

efficiency has been compromised somewhat in favor of effective, low-hinge-moment wing-tip ailerons. (See reference 2.) Compensation for the low aerodynamic damping associated with the low-aspect-ratio delta wing must depend on autopilot design. The only performance specifications imposed on the roll stabilization systems are that roll-angle changes (due to the expected disturbing roll torques) were not to exceed 10° from the reference roll attitude, and that the autopilots considered have proportional static characteristics. All other performance characteristics are judged on a comparative basis. Maximum control-surface deflections were limited to $\pm 10^{\circ}$ on each aileron.

Since the airframe requires roll stabilization only and the autopilot is not to be a control element, the airframe-autopilot system acts as a regulator, and was analyzed accordingly. The analysis was conducted and a satisfactory roll-autopilot design determined analytically on the basis of estimated airframe aerodynamic and inertia characteristics, available experimental autopilot data, and calculated autopilot component characteristics. Effects of variations in the aerodynamic damping and rolling inertia were considered in the analysis. System operation at two altitudes and Mach numbers was determined. In general form the methods of analysis and design presented herein apply also to pitch and yaw stabilization.

SYMBOLS

δ_a total differential aileron deflection, degrees

$L_{\dot{\phi}}$ rolling-moment variation with rolling velocity, foot-pounds per radian/second $(\partial L/\partial \dot{\phi})$

L_{δ_a} rolling-moment variation with aileron deflection, foot-pounds per radian $(\partial L/\partial \delta_a)$

q dynamic pressure, pounds per square foot

S wing area, square feet

b wing span, feet

V velocity, feet per second

ϕ roll attitude, degrees

$\dot{\phi}$ rate of roll, radians per second $(d\phi/dt)$

ϕ_o system roll-position output, degrees

K control gearing ratio; value of $\delta a/\phi(j\omega)$ at $\omega = 0$; static autopilot gain

K_r rate-gyro static sensitivity; value of $\delta a/\dot{\phi}(j\omega)$ at $\omega = 0$; degrees per degree per second

C_{l_p} roll damping-coefficient derivative $\left(L_{\dot{\phi}}/qSb\,\frac{b}{2V}\right)$

$C_{l_{\delta_a}}$ control moment-coefficient derivative $\left(L_{\delta_a}/qSb\right)$

L_d moment due to a roll disturbance in equivalent degrees of δ_a $\left(\text{unit } L_d = \frac{L_{\delta_a}}{57.3}\right)$

ω frequency, radians per second

D differential operator (d/dt)

M Mach number

I_X moment of inertia about the body center line, slug-feet square

$j = \sqrt{-1}$

DESCRIPTION OF AIRFRAME-AUTOPILOT SYSTEMS CONSIDERED

Airframe

The airframe requiring automatic roll stabilization is shown in figure 1. The jet engines provide thrust for the "cruising" portion of the flight. The wing-tip control surfaces are to be used as ailerons only. The canard fins are to provide pitch and yaw control.

Airframe-Autopilot Systems

Gyro-actuated roll stabilization system.- The initial autopilot choice was one of maximum simplicity that had been found capable of stabilizing another pilotless aircraft with similar stabilization

requirements. While it would not be expected that the same autopilot would give satisfactory performance "as is" in a new airframe and under differing flight conditions, minor adjustments might adapt the autopilot to the new system. The autopilot described in reference 2 was investigated first. This system couples a position gyroscope outer gimbal directly to the ailerons through a simple linkage. Thus the aileron deflections are proportional to the roll attitude change measured by the gyroscope.

Gyro-actuated control with rate.- This system includes the gyro-actuated control and a rate-sensing device. In figure 11 of reference 3, an experimentally determined response of a rate gyro-pneumatic servomotor combination is presented. The pneumatic servomotor valve is positioned by the rate gyroscope gimbal and a feedback linkage from the servo shaft. The servo output therefore is proportional to angular velocity sensed by the rate gyro, when $\omega = 0$.

Since symmetrical aileron motion is desired, the outputs of the position- and rate-sensing elements must be added and then differentially applied to the ailerons. This system is seen to require a complex mechanical linkage to retain symmetry of aileron motion.

Electronic-hydraulic autopilot.- An autopilot consisting of a direct-current amplifier, solenoid-operated hydraulic valve, and hydraulic servomotor was available for bench testing. This amplifier-servomotor combination may be used with any type of motion-sensing device which will relay a suitable signal to the amplifier. Motion sensing devices would include position and rate gyroscopes, angular and linear accelerometers, and altitude and angle-of-attack sensing instruments. A position gyroscope was chosen as the sensing instrument to be used in this autopilot because of availability and because position stabilization of the airframe is desired.

The electronic-hydraulic autopilot is more complex than the systems previously considered and is at an additional disadvantage when compared to the gyro-actuated control because of the hydraulic power supply required. The outstanding advantage of this electronic-hydraulic autopilot is that its characteristics may be altered readily by use of passive electrical networks, thereby adapting it to wide ranges of operation. The hydraulic servomotor is also adaptable to wide ranges of force output.

SYSTEM ANALYSIS PROCEDURE

Combination of Airframe and Autopilot

In many applications, pilotless aircraft must be roll-stabilized in order to allow proper operation of control components governing the pitching and yawing motions. The function of the roll stabilization system is to counteract rolling torques applied to the airframe and to maintain a reference within acceptable limits. Rolling torques may arise because of construction asymmetry and thrust misalinement, gusts, or aerodynamic coupling between pitching and yawing motions. In system analyses, then, the motion to be investigated is the response of the system to rolling torques applied to the airframe. The manner of application of the disturbance is important to the analysis since the system response would differ with the method of disturbance. A "command" input, ϕ_i, to the autopilot, for instance, might produce a different system response than an applied roll torque, even though both disturbances are applied to the system with the same time variation and are of equivalent magnitudes.

The following block diagram describes the system in its most simple form as a servomechanism:

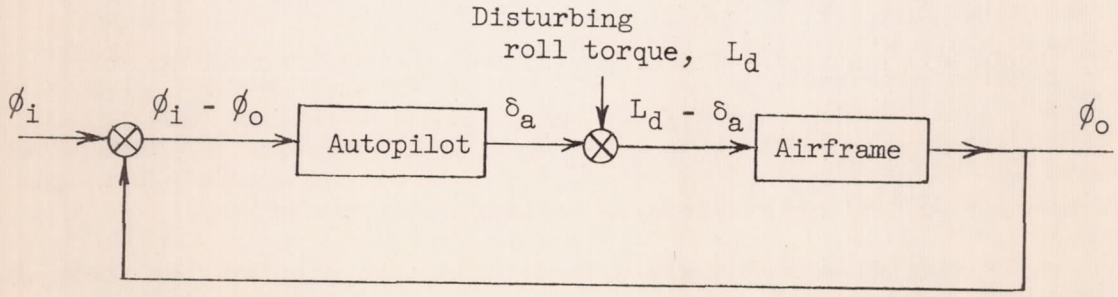

Since the complete roll stabilization system may be activated prior to flight and there is to be no ϕ_i ("command" input to the autopilot), but roll torque disturbances are expected, the system acts as a regulator according to the definitions of reference 4.

For $\phi_i = 0$, the block diagram may be redrawn:

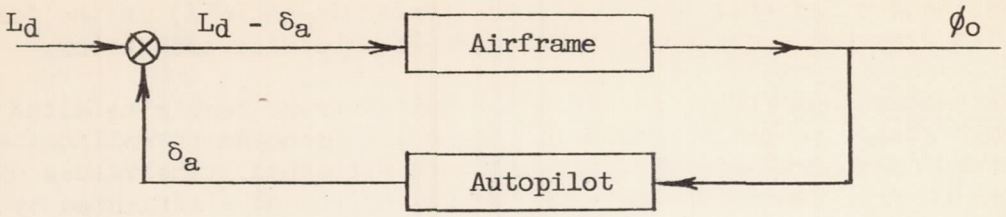

System analyses would be valid using either of the two block diagrams. However, the latter diagram points out that the autopilot will be, effectively, in the feedback loop when the system roll-position response to an applied roll torque ϕ_o/L_d is considered. System frequency responses $\phi_o/L_d(j\omega)$ were determined in accordance with these diagrams, and transient responses to the anticipated disturbing roll torques L_d were determined from the $\phi_o/L_d(j\omega)$ responses by a Fourier series technique.

Determination of Airframe Frequency Responses

Frequency response.- The single-degree-of-freedom roll equation

$$I_X D^2\phi - L_{\dot{\phi}} D\phi = L_{\delta_a}\delta_a$$

was assumed to define the airframe rolling characteristics.

The preceding equation may be rewritten as:

$$\frac{\phi}{\delta_a}(D) = \frac{\dfrac{L_{\delta_a}}{-L_{\dot{\phi}}}}{D\left(\dfrac{D}{\dfrac{-L_{\dot{\phi}}}{I_X}} + 1\right)}$$

In this form, the frequency response may be plotted directly by substituting $D = j\omega$ and employing the graphical method given in article 3, chapter 8, of reference 4. Frequency-response calculations for a specific subsonic airframe are described in some detail in reference 5.

An airframe frequency response as plotted from the $\phi/\delta_a(j\omega)$ response equation is shown in figure 2. Figure 3 presents the frequency responses determined (for the conditions listed in table I) in the form of Nyquist diagrams. The Nyquist diagrams will be discussed later.

Derivatives and flight conditions.- The airframe requiring automatic roll stabilization is shown in figure 1. Aerodynamic rolling derivatives and inertia of the airframe were estimated. The values of the aileron-control-effectiveness derivative $C_{l_{\delta_a}}$ were estimated by extrapolation of data found in references 2 and 6. The variation of the damping derivative C_{l_p} of the horizontal wings with Mach number was assumed to be the same as that of the wings of references 2 and 6 and their damping was estimated by extrapolation of the data found in these references. The vertical wings include jet engines and the engine supports, and are assumed to contribute less damping than the horizontal wings. The damping of the horizontal wings was arbitrarily increased by 75 percent to allow for the contribution of the vertical wings. The estimated inertia and aerodynamic parameters for the chosen flight conditions are listed in table I, and are discussed in the following paragraphs.

Some variations in the constants appearing in the preceding equation were investigated to determine the effect of these variations on the airframe frequency response.

The conditions listed in table I assumed that the pilotless aircraft may operate at Mach numbers increasing from 2 to 2.5 at altitudes from 20,000 feet to 40,000 feet. The two flight conditions chosen ($M = 2$ at 20,000 feet, and $M = 2.5$ at 40,000 feet) were assumed to be the extreme operating limits for this analysis.

The airframe inertia was varied from the estimated maximum to the estimated minimum to determine its effect on the airframe response characteristics. The effect of this variation may be seen in the Nyquist diagram of figure 3(a). In the system analyses that follow, the airframe response for the 20,000-foot flight condition was calculated using the lower value of I_X, and the 40,000-foot response with the higher I_X value.

The aerodynamic damping was reduced to 50 percent of the estimated values of $L_{\dot{\phi}}$ to determine the effect on the airframe frequency responses of a possible large over-estimate of $L_{\dot{\phi}}$. The Nyquist diagrams of figure 3(b) show the effect of decreased damping on the airframe frequency response. The estimated values of $L_{\dot{\phi}}$ were used in the following system analyses.

Figure 3(c) shows the Nyquist plots for the chosen flight conditions and are the airframe frequency responses used in system analyses.

For the single-degree-of-freedom airframe rolling characteristics, the semi-log plots similar to figure 2 may also be used in lieu of Nyquist diagrams. When the significance of the Nyquist diagram is understood, the useful features of the polar plot are easily recognized on the semi-log plot. Gain changes desired and comparison of airframe response variations with altitude, Mach number, and other parameter changes may be determined directly without recourse to additional polar plotting.

Autopilot-Frequency-Response Determination

Gyro-actuated control.- The frequency response of the gyro-actuated autopilot has been shown by bench and flight tests (see reference 2) to be a constant amplitude ratio and constant (0°) phase angle over the frequency range of interest. The amplitude ratio of this autopilot may be adjusted by changing the mechanical gearing between the gyro and ailerons. The frequency response of the gyro-actuated control is described by the constant K which may assume any value consistent with the limitations imposed by the mechanical linkage.

Gyro-actuated control with rate.- The system block diagram including the rate servo may be drawn as follows:

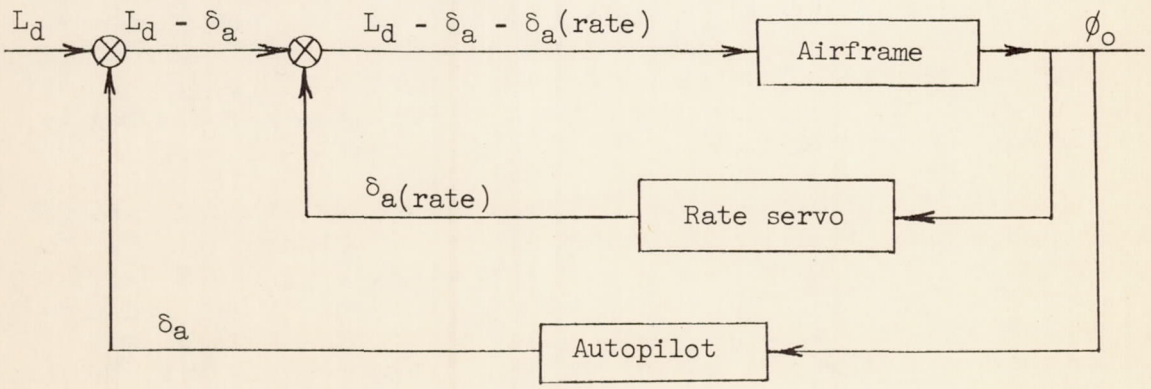

The diagram indicates that for purposes of analysis the autopilot and rate-servo frequency responses are introduced separately. The rate-servo frequency response was determined experimentally for $K_R = 0.1$. The system frequency response may be adjusted by varying either K or K_R.

Electronic-hydraulic autopilot.- The experimentally determined frequency response of this autopilot is shown in figure 4. The calculated effect on the frequency response of adding a passive electrical lead network in cascade with the autopilot is also shown in the figure. The lead network is described in a subsequent section of this paper.

The gain of this autopilot may be varied by changing the level of the voltage applied to the amplifier. The autopilot frequency response may be varied by changing the lead network.

System Frequency Responses

Combination of airframe and autopilot.- The next step in the analysis procedure is the determination of the complete system frequency response of roll position to a roll torque disturbance $\phi_o/L_d(j\omega)$. This response is related to the frequency responses of the airframe and autopilot, as follows:

$$\frac{\phi_o}{L_d}(j\omega) = \frac{\left[\frac{\phi}{\delta_a}(j\omega)\right]_{\text{airframe}}}{1 + \left[\frac{\phi}{\delta_a}(j\omega)\right]_{\text{airframe}}\left[\frac{\delta_a}{\phi}(j\omega)\right]_{\text{autopilot}}}$$

A graphical maneuver simplifies the computation of $\phi_o/L_d(j\omega)$. The M-N contour chart, which is a Lm-angle chart with M-N contours superimposed, and of which figure 5 is an example, allows the closed-loop function $\delta_a/L_d(j\omega)$ to be read directly from the curved contours when the product of $\left[\phi/\delta_a(j\omega)\right]_{\text{airframe}}$ and $\left[\delta a/\phi(j\omega)\right]_{\text{autopilot}}$, the open-loop frequency response, is plotted on the rectangular coordinates. (Further information on the use of the M-N contour chart may be found in chapter 8 of reference 4.) The function $\phi_o/L_d(j\omega)$ may then be determined from $\frac{\delta a}{L_d}(j\omega)\frac{1}{\left[\frac{\delta_a}{\phi}(j\omega)\right]_{\text{autopilot}}}$. Since the amplitude responses of $\delta_a/L_d(j\omega)$ and $\left[\delta_a/\phi(j\omega)\right]_{\text{autopilot}}$ are expressed in decibels (db), both the amplitude and phase of $\left[\delta_a/\phi(j\omega)\right]_{\text{autopilot}}$ may be subtracted from the amplitude and phase of $\delta_a/L_d(j\omega)$ to determine the roll position frequency response to a roll torque disturbance $\phi_o/L_d(j\omega)$. Several plots of $\phi_o/L_d(j\omega)$ are presented in figure 6(c) in connection with the system analysis.

The response of $\delta_a/L_d(j\omega)$ is also of interest; it is the control-surface dynamic response to the roll torque disturbance, and must be considered so that maximum available control-surface deflections may be set on the basis of the deflections required to correct for the expected disturbance and out-of-trim moments. Maximum hinge-moment estimates may be based on these deflections.

System including the gyro-actuated control.- Frequency responses were determined for the airframe and gyro-actuated control system according to the procedure outlined in the preceding section.

Open-loop frequency responses of the airframe and gyro-actuated control with $K = 1$ as determined on the semi-log graph paper are shown in figure 6(a). Figure 6(b) shows the system open-loop frequency responses for various values of control gearing ratio, K. Figure 6(c) shows the closed-loop frequency responses corresponding to the open-loop responses of figure 6(b).

System including the gyro-actuated control and rate.- The analysis of this system requires that the closed-loop frequency response of the inner loop (consisting of the airframe and the rate-servo) be determined; the method previously presented for the determination of over-all system frequency responses is applicable. The over-all system response may then be determined by the use of the inner-loop closed-loop frequency-response characteristics to represent the dotted box in the following block diagram:

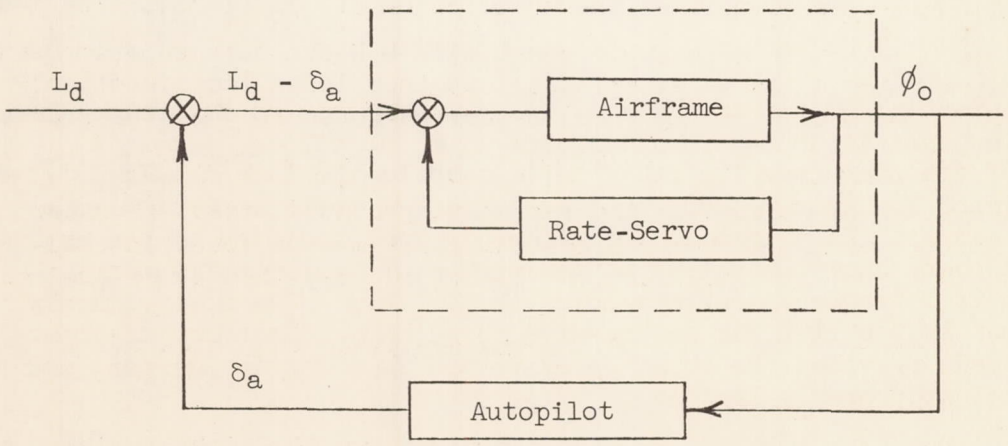

The system closed-loop response $\phi_o/L_d(j\omega)$ may then be determined from

$$\frac{\phi_o}{L_d}(j\omega) = \frac{\frac{\phi_o}{L_d - \delta_a}(j\omega)}{1 + \frac{\phi_o}{L_d - \delta_a}(j\omega)\frac{\delta_a}{\phi}(j\omega)}$$

which is of the same form as the previously discussed closed-loop system responses.

Open-loop frequency responses of the inner loop are shown on the M-N contour chart of figure 7(a). The curves of figure 7(b) corresponding to $K = 1$ (no gain adjustment) represent the closed-loop frequency responses of the inner loop, as well as the system open-loop frequency responses. Figure 7(c) presents the closed-loop frequency responses corresponding to the open-loop curves of figure 7(b) with a gain adjustment of 6.5 decibels ($K = 2.1$).

System including the electronic-hydraulic autopilot.- The system (no lead network) open-loop frequency response for the 40,000-foot flight condition is shown on the M-N contour chart of figure 8(a). The corresponding closed-loop frequency response is shown in figure 8(b). A discussion on inclusion of a lead network in the system frequency response is given in the section entitled "DETAILED DESIGN PROCEDURE."

Transient-Response Determination

The remaining step in the analysis procedure is to determine the system response to an input disturbance as a function of time. A method of transfer from the frequency domain to the time domain is given in reference 7. This method requires the input to be expressed as a Fourier series. Each term in the series is then modified by the amplitude and phase characteristics of the system closed-loop frequency response at a frequency corresponding to the term. The most commonly used input is the step, or square-wave form. Any other form of input may be used, provided the input is expressed as a Fourier series, and the method is properly applied.

A "ramp" function (input magnitude proportional to time) was chosen as the type of input best describing the roll-torque disturbances (due to the build-up of angle of attack and/or sideslip when maneuvering) expected to be applied to this system. The "ramp" function wave form

is sketched below:

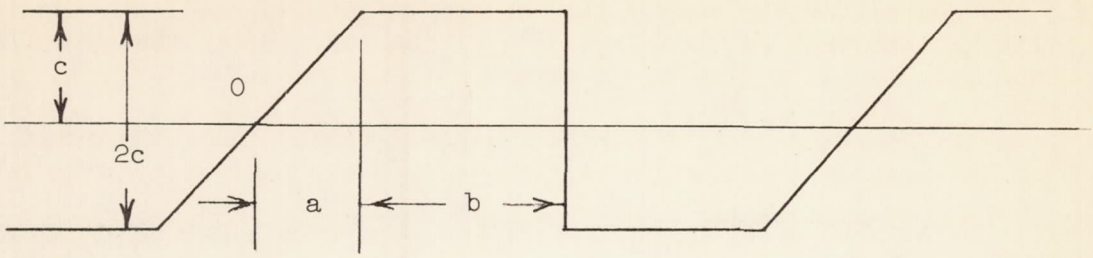

The series describing this wave form is:

$$f(t) = 2c \sum_{n=1,2}^{\infty} \left[\frac{a + b}{an^2\pi^2} \sin\left(\frac{n\pi a}{a + b}\right) + \frac{(-1)^{n+1}}{n\pi} \right] \sin\left(\frac{n\pi t}{a + b}\right)$$

where a, b, and c, are defined in the sketch, time is measured from the point 0, and n is the number of the term, or harmonic, in the series. The values of a used are representative of the build-up time of angle of attack or sideslip that may be expected to induce rolling moments for the respective flight conditions. The value of b was varied with the system response considered. The value of c chosen was 0.5 (2c = 1) for all inputs. The number of harmonics (equal to the number of terms) was fixed at 24 for all transient-response calculations presented in this paper because a Fourier synthesizer incorporating components for 24 harmonics was available for automatic summation of the series. The input curves as determined from the synthesizer for the two flight conditions are shown in figure 9.

When the form of the input had been established, the system characteristics were superimposed on the input series by inserting the amplitude ratio R and the phase angle PA in the series expression as follows:

$$f(t) = 2c \sum_{n=1,2}^{24} \left[\frac{a + b}{an^2\pi^2} \sin\left(\frac{n\pi a}{a + b}\right) + \frac{(-1)^{n+1}}{n\pi} \right] R \sin\left(\frac{n\pi t}{a + b} + PA\right)$$

where the amplitude ratio and phase angle were read from the system closed-loop frequency response at the frequency $\frac{n\pi}{a + b}$ radians per second.

The system response to the abrupt step portion of the input wave form is of interest as the most taxing disturbance that may be applied to the system. While such a disturbance is not expected, the possibility exists that gust conditions or irregularities in the autopilot components may give rise to an abrupt rolling moment.

The following conditions or characteristics which are apparent from the transient motion are desired of the airframe-autopilot system:

(a) A fast, well-damped transient response to a disturbing roll torque.

(b) A relatively high control gearing ratio δ_a/ϕ in the steady-state ($\omega = 0$) condition, which is equivalent to a small roll position change due to a disturbing roll torque.

(c) The preceding conditions must hold for the entire range of flight conditions to be encountered.

DETAILED DESIGN PROCEDURE

The purpose of this portion of the paper is to present the procedures employed in attempts to adapt the existing autopilot equipment previously discussed to the present roll stabilization requirements.

The design procedure leans heavily on an understanding of the significance of the graphical analysis procedures. The effects of adjustments to the system open-loop plots on the M-N contour charts in terms of the resulting changes in the closed-loop responses may readily be approximated without determination of the entire closed-loop responses. The system transient characteristics may also be deduced from careful examination of the system closed-loop frequency responses.

Airframe and gyro-actuated control.- The analysis of this system showed that, for unit static control gearing, an oscillatory system response might be expected. The only autopilot adjustment that would affect the system response characteristics is a change in gain K. The value of gain was, therefore, reduced from unity to 0.1. The system dynamic response was improved somewhat, but the static control gearing was too low to be tolerated. System responses were also determined for $K = 2$, to ascertain the system dynamic characteristics with a desirable value of static control gearing. The system closed-loop frequency responses for the three values of gain may be compared in figure 6(c). These closed-loop responses all indicate oscillatory transient characteristics. Although the shape of the closed-loop

frequency-response curves may be improved thereby, further gain reduction below $K = 0.1$ would result in unacceptable static characteristics. The conclusion is reached that the gyro-actuated control is not adaptable to roll stabilization of the airframe under the expected flight conditions.

Airframe, gyro-actuated control and rate-servo.- The addition of the rate-servo to the airframe and gyro-actuated autopilot system changed the shape of the system open-loop frequency response curves (see figure 7(b)). A rate-gyro sensitivity K_r of 0.1 was found to result in satisfactory system response characteristics when the gyro-actuated autopilot gain was adjusted 6.5 decibels ($K = 2.1$). The adjusted system closed-loop frequency-response curves for the extreme flight conditions are shown in figure 7(c).

The physical inclusion of the rate-servo in the system is an integral part of the system design. To retain symmetry of aileron motion, it is necessary to add the outputs of the gyro-actuated autopilot and the rate-servo and to deliver these outputs to the ailerons as equal differential displacements. This may be accomplished with a relatively complex mechanical linkage.

Airframe and electronic-hydraulic autopilot.- The open-loop frequency response of the airframe and electronic-hydraulic autopilot system for the 40,000-foot flight condition is shown in figure 8(a). Obviously, some phase lead must be introduced in order to produce a satisfactory airframe-autopilot system response. Phase lead may be built into this system by modifying the electrical signals in the autopilot with suitable networks. There are many passive electrical networks described in electronics literature that may be used with an electrical system to introduce phase lead or lag, signal gain changes, and corresponding operating frequency changes. One such network is shown in figure 22, p. 268 of reference 4. This network is simple, consisting of two resistors and a condenser, and is extremely versatile. Variations of the value of the components of this network will adjust phase lead, amplitudes, and frequencies at which the network is most effective.

An examination of the airframe-plus-autopilot (no lead network) response on the M-N contour graph paper, figure 8(a), and of the previously discussed graphical procedure involved in determining the system closed-loop frequency response to a disturbing roll torque, indicate that excessive increases in gain and phase lead would be undesirable. That is, the graphical procedure involves determination of the frequency response of aileron deflection to a roll torque disturbance $\delta_a/L_d(j\omega)$, and then division of the $\delta_a/L_d(j\omega)$ response by the frequency response of aileron deflection to roll attitude change, $\delta_a/\phi(j\omega)$. Since

$\delta_a/\phi(j\omega)$ included the characteristics of the lead network as well as those of the autopilot,

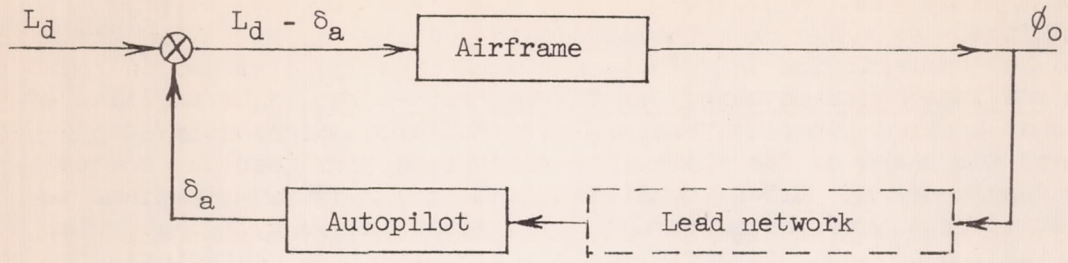

excessive phase lead and increased gain in this response will result in an overdamped, low-frequency-range closed-loop frequency response, indicating a slow transient response. An example of this is illustrated in figure 10. Figure 10(a) shows the open-loop response of the system including an experimentally determined (autopilot and lead network) frequency response. The system stability appears satisfactory, but the closed-loop frequency response shown in figure 10(b) is not satisfactory, since a slow transient response is indicated. In order to improve the system response, it is necessary to change the autopilot characteristics such that the end response is as desired with only secondary consideration for the amount of system stability. That is, the degree of system stability is not apparent from an examination of the system open-loop frequency response. An examination of figure 10(a) shows one effect of excessive phase lead. Shifting the locus to the right on the figure results in a decreased amplitude response of $\delta_a/L_d(j\omega)$ read from the closed-loop contours on the figure. A further excessive decrease results when the large phase-lead and corresponding amplitude characteristics of the autopilot with lead network are removed from the $\delta_a/L_D(j\omega)$ response as previously described to yield the closed-loop frequency response characteristics.

From the above discussion, it may be seen that the response of $\delta_a/L_d(j\omega)$ must appear rather underdamped, so that the resulting closed-loop system frequency response will not be overdamped. The characteristics of the lead network should be such that the $\delta_a/L_d(j\omega)$ peak must be greater (by a rule-of-thumb factor of 1 to 1.3 times the $\omega = 0$ system closed-loop amplitude response ϕ_o/L_d) than the autopilot and lead network amplitude response δ_a/ϕ at the frequency corresponding to the δ_a/L_d frequency-response peak. Compliance with this requirement is not too difficult for a given condition; the lead network may readily be changed in a manner to produce the desired characteristics.

Difficulty does arise in meeting this requirement (and the other desired characteristics previously listed) simultaneously for both extreme flight conditions considered.

It is desirable from the standpoint of simplicity to fix the autopilot characteristics $\delta_a/\phi(j\omega)$ for all flight conditions. A compromise in the system responses for various flight conditions was reached, so that a fixed autopilot characteristic, while not capable of producing an optimum response for all flight conditions, produced an acceptable response under all flight conditions and a near-optimum response over a large portion of the expected flight path. However, large variations in flight conditions may require that the autopilot characteristics be changed with Mach number or altitude, or both. Usually changes in autopilot gain will suffice to adjust the system response for various conditions encountered along an expected flight path. Auxiliary autopilot equipment may be installed in the airframe if it should become necessary to provide continuous or incremental gain adjustment as flight conditions change.

The preceding considerations resulted in the choice of a lead network that does not contribute an excessive amount of phase lead. Figure 11(a) shows the system open-loop frequency responses calculated for the two extreme flight conditions using a lead network in cascade with the autopilot. The lead network is defined by $\alpha = 3$ and $\omega_1 = 5$, where $\alpha = \frac{R_1 + R_2}{R_2}$ and $\omega_1 = \frac{1}{R_1 C}$ in the following sketch:

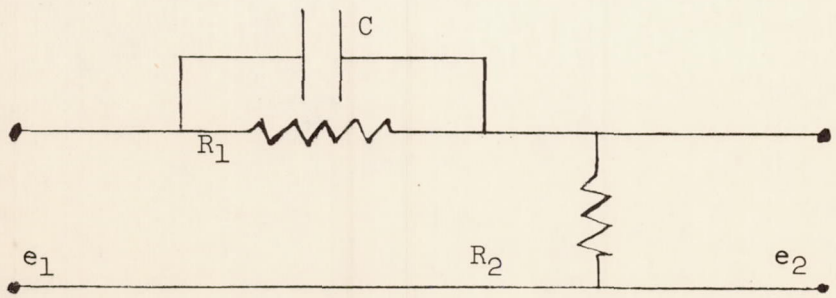

The calculated effect of this lead network on the autopilot frequency response may be seen in figure 4.

The autopilot gain was assumed to be adjusted to give the equivlent of a lead network response of unity at $\omega = 0$. This may be

accomplished physically by increasing the voltage at the gyro potentiometer pickoff by a factor equal to α. The network response is then:

$$\alpha\frac{e_2}{e_1}(j\omega) = \frac{\frac{j\omega}{\omega_1} + 1}{\frac{j\omega}{\alpha\omega_1} + 1}$$

Figure 11(c) shows the system transient responses (corresponding to the closed-loop frequency responses of figure 11(b)) to the ramp inputs for both flight conditions. The response to the step portion of the input is seen to be somewhat slow. The autopilot control-gearing ratio δ_a/ϕ in the steady-state ($\omega = 0$) condition is unity for the system of figure 11. It is desirable to increase both the speed of the system response and the ratio δ_a/ϕ at $\omega = 0$.

Previous experience with the system has shown that increased gain in the open loop increases the system operating frequency. Increased gain is a direct result of increasing the control-gearing ratio. Thus the basic requirements for the desired improvements in the system response are compatible. However, the system response with the $\alpha = 3$, $\omega_1 = 5$ lead network is not well-adapted to changes in gain. The "bucket" (low-frequency range amplitude response less than the $\omega = 0$ amplitude response) shown in the curves of figure 11(b) contributes to the slow system response. Rough checks at a few frequency points of the adjusted open-loop response curve indicated that the desired gain adjustment alone would not remove the bucket. Examination of the autopilot-airframe (no lead network) closed-loop frequency response shown in figure 8(b) indicates that the bucket is caused by the lead network. A change in the network in the frequency range up to the system operating frequency would probably reduce or eliminate the bucket. Increasing the value of ω_1 was found to result in a change in the desired direction. Figure 12(a) shows the system open-loop responses with the lead network $\alpha = 3$ and $\omega_1 = 50$. Figure 12(a) also shows the curves for the open-loop responses with a gain adjustment of 12 decibels. The closed-loop responses of the system with the adjusted gain are shown in figure 12(b). (The 12-db gain corresponds to a control-gearing ratio δ_a/ϕ of 3.98, which is desirable.) However, the $\alpha = 3$, $\omega_1 = 50$ network represents an over-correction of the previously discussed bucket condition; the high (compared to the $\omega = 0$ amplitude) values of the closed-loop peak amplitude responses of figure 12(b) indicate oscillatory transient responses for both flight conditions. Some additional increase in system gain would tend to reduce the magnitudes of the peaks in the $\phi_o/L_d(j\omega)$ responses, would increase the speed of the system transient responses, and would increase

the control-gearing ratio. Unfortunately, there are physical limitations to discourage extremely high gains. Chief among these limitations is the possibility of autopilot amplifier saturation. Another limitation (dependent on the lead-network effect and the gain adjustment) is in the resulting control-surface deflections. As stated previously, the response read from the closed-loop contours of the M-N contour graph is the response of $\delta_a/L_d(j\omega)$. Examination of figure 12(a) (gain adjusted 12 db) shows a peak in the $\delta_a/L_d(j\omega)$ response of 11 decibels for the 40,000-foot flight condition. This peak is indicative of a large over-shoot in the transient response of aileron deflection to a disturbing roll torque and a large control-surface deflection means more stringent autopilot servomotor requirements.

It is apparent that characteristics approaching those desired of the system may be realized with a lead network between the $\alpha = 3$, $\omega_1 = 5$ network and the $\alpha = 3$, $\omega_1 = 50$ network.

System frequency responses are shown in figures 13 and 14, with lead networks described by $\alpha = 3$, $\omega_1 = 15$ and $\alpha = 3$, $\omega_1 = 20$, respectively. The system of figure 13 has a gain adjustment of 8 decibels, while that of figure 14 has a gain adjustment of 13 decibels. A comparison of figures 13(b) and 14(b) shows that while either pair of closed-loop responses represents a good compromise of gain adjustment over the expected range of flight conditions, the system with the $\alpha = 3$, $\omega_1 = 20$ network results in higher operating frequencies and higher static control gearing. As previously stated, difficulties may be encountered in adjusting the autopilot to high values of gain. The 13-decibel gain adjustment required to produce the responses of figure 14 may not be physically realizable. The system of figure 13 is physically realizable. It may be concluded that either the more desirable system of figure 14 or the satisfactory system of figure 13 will result in satisfactory roll-stabilization characteristics with fixed gain over the range of flight conditions.

RESULTS AND DISCUSSION

Airframe and gyro-actuated control system.- The proved capabilities and simplicity of the gyro-actuated autopilot point out the advantages of this system where a no-lag roll-stabilization autopilot is adequate. Unfortunately, the gyro-actuated control is also a no-lead autopilot; that is, the frequency response of this autopilot is a constant amplitude ratio and constant (0°) phase angle for the frequency range in which it has been tested, and its physical make-up is such that only the static gain (ratio of δ_a/ϕ at $\omega = 0$) may be adjusted. Maximum gains are limited by autopilot physical characteristics such as cam slope

(mechanical advantage) and force output available. Minimum gains are limited by the allowable variation in roll position of the airframe under consideration.

In the course of the design procedure, it was seen that the autopilot gain would have to be reduced to $K = 0.1$ to improve the degree of system stability noticeably. This gain reduction means that δ_a/ϕ in the steady state is 0.1, or that the airframe must roll 10° to enable the autopilot to produce 1° of correcting aileron deflection. The maximum disturbing roll torque to be encountered by this airframe is estmated to be equivalent to 4° of aileron deflection. Maximum out-of-trim rolling moment due to construction assymetry is estimated to be equivalent to 2° of aileron deflection. The sum of these two rolling moments would cause the imperfectly stabilized airframe to roll to an angle of 60° in the steady-state condition. This change in roll position is excessive. For this airframe, roll-position variations of less than $\pm 10^\circ$ are desired. In addition to poor static characteristics, the responses of figure 6(c) indicate undesirable dynamics for the system with $K = 0.1$ as well. The resonant frequencies are low, indicating low system operating frequencies and the peak amplitudes indicate that even with this low K, the system responses would be somewhat oscillatory.

The system transient responses $\phi_o/L_d(t)$ were determined from the Fourier synthesizer for the airframe and gyro-actuated control system. Responses with $K = 1$ and $K = 2$, more practical values of control gearing, are shown in figure 15. These responses confirm the conclusions based on the closed-loop frequency responses. The poor system static characteristics with greatly reduced gain and the oscillatory transient responses for all practical values of control gearing K combine to make this autopilot unsatisfactory for all values of gain.

Airframe, gyro-actuated control, and rate servo.- The rate servo was added to the airframe and gyro-actuated control system to introduce additional damping, thereby improving the system response characteristics. Transient responses of this system corresponding to the closed-loop frequency responses of figure 6(c), are shown in figure 16. These transient responses are satisfactory. The 6.5-decibel gain adjustment corresponds to a control gearing ratio of 2.1, so system static characteristics are satisfactory. The peaks in the $\delta_a/L_d j\omega$ responses do not exceed 2 decibels, indicating that aileron deflections would be held to small values.

There are several features of this system that must be considered in addition to the characteristics just discussed. The sensitivity adjustment of the rate-servo requires a considerable amount of time and skill. The linkage required to perform the addition of the rate

and position outputs and to transform these outputs into differential aileron deflections would be of a complex design and difficulties would certainly be encountered in assembly. These mechanical difficulties, while not insurmountable, contribute to render this an undesirable system.

Airframe and electronic-hydraulic autopilot.- Because of the mechanical difficulties discussed in the previous section, the advantages of the electronic-hydraulic autopilot are more easily appreciated. Effective damping may be introduced into this system readily, and the linkage between the hydraulic servomotor and the control surfaces may be quite simple.

Figures 17 and 18 show the system transient responses to the ramp inputs corresponding to the closed-loop frequency responses of figures 13(b) and 14(b), respectively. Either of the two systems is acceptable from the standpoint of response characteristics. The detailed design section of this paper pointed out that the gain adjustment of 13 decibels applied to the system of figure 18 is the more desirable from the standpoint of static control gearing, but the required gain may not be physically realizable for the existing autopilot and the lead network. The 8-decibels gain adjustment applied to the system of figure 17 is physically realizable and the resulting control gearing is acceptable. The peaks in the $\delta_a/L_d j\omega$ response of figure 13(a) for the $\alpha = 3$, $\omega_1 = 15$ system do not exceed 6.5 decibels, which is a ratio of 2.1. For the $\alpha = 3$, $\omega_1 = 20$ system, the $\delta_a/L_d(j\omega)$ peaks (fig. 14(a)), do not exceed 7.5 decibels, which is a ratio of 2.4. On the basis of the previously mentioned estimates of out-of-trim moments and applied rolling disturbances, the maximum control-surface deflections required for the systems of figures 11 and 12 would be less than 10.4° and 11.6°, respectively. Original estimates of maximum control-surface deflections for the airframe used in preliminary hinge-moment estimates were $\pm 20^\circ$, so either of these two systems would allow a large margin of safety over initial estimates.

In spite of the uncertainty connected with the high gain corresponding to the system characteristics shown in figure 18, these responses remain an important part of the analysis. In the building and subsequent testing of the two networks, it may be found that the networks will not have exactly the characteristics described by the mathematical representation presented earlier. Decreased amounts of phase lead in the experimentally determined network response characteristics may cause the $\alpha = 3$, $\omega_1 = 15$ network to have an effect on the system response similar to that computed for the $\alpha = 3$, $\omega_1 = 5$ network; the $\alpha = 3$, $\omega_1 = 20$ network may, by the same token, require a smaller system gain adjustment than the analysis indicates.

Availability of network components may result in a network described by $\alpha = 3.1$, perhaps. A suitable gain adjustment might then be made to produce acceptable system responses. The addition to the autopilot of one of these two networks with suitable gain adjustment will result in a satisfactory roll autopilot for the airframe, under the expected flight conditions.

Contribution of method of analysis to system design.- The design procedures employed in the choice of a suitable lead network to be used with the electronic-hydraulic autopilot illustrate the value of the graphical methods of analysis. While an initial trial-and-error approach is required, the effects of parameter changes on the curve shapes soon lead to "educated guesses" and finally result in a direct approach to the design required to produce the desired system responses. The graphs are especially useful in simultaneous design for two flight conditions; the effect of parameter changes on both curves may be checked quickly and unsuitable combinations discarded without wasted effort.

CONCLUSIONS

The system analyses and autopilot design considerations presented lead to the following conclusions:

1. The electronic-hydraulic autopilot with a suitable passive electrical lead network will provide satisfactory system response characteristics over the expected range of flight conditions with fixed gain. No difficulties are anticipated in adding the lead network to the autopilot. This autopilot appears to meet all the requirements for roll stabilization of the airframe and is considered suitable for flight testing.

2. The graphical procedures employed in system analyses provide an insight into the effect of parameter variations on the system characteristics and indicate a direct approach to system design.

3. The airframe rolling characteristics under the expected flight conditions require autopilot characteristics beyond the range of adjustments that may be made to the gyro-actuated control. The gyro-actuated control is not a satisfactory autopilot for the airframe under consideration.

4. The addition of the rate gyro-pneumatic servo to the airframe and gyro-actuated control allows adjustments of both control components to be made which result in good system response characteristics for both extreme flight conditions. However, this autopilot arrangement

is not considered desirable because of the mechanical complexities involved in adding the outputs of the autopilot components.

Langley Aeronautical Laboratory
National Advisory Committee for Aeronautics
Langley Field, Va.

REFERENCES

1. Mc Cabe, A. P.: Induced Rolling Moments on the Nike and Sparrow Missiles. Rep. No. SM-13795, Douglas Aircraft Co., Inc, July 19, 1950.

2. Gardiner, Robert A., and Zarovsky, Jacob: Rocket-Powered Flight Test of a Roll-Stabilized Supersonic Missile Configuration. NACA RM L9K01a, 1950.

3. Nelson, Walter C., and Passera, Anthony L.: A Theoretical Investigation of the Influence of Auxiliary Damping in Pitch on the Dynamic Characteristics of a Proportionally Controlled Supersonic Canard Missile Configuration. NACA RM L50F30, 1950.

4. Brown, Gordon S., and Campbell, Donald P.: Principles of Servomechanisms. John Wiley & Sons, Inc., 1948.

5. Gardiner, Robert A., Zarovsky, Jacob, and Ankenbruck, H. O.: An Investigation of the Stability of a System Composed of a Subsonic Canard Airframe and a Canted-Axis Gyroscope Automatic Pilot. NACA TN 2004, 1950.

6. Martz, C. William, and Church, James D.: Flight Investigation at Subsonic, Transonic, and Supersonic Velocities of the Hinge-Moment Characteristics, Lateral-Control Effectiveness, and Wing Damping in Roll of a 60° Sweptback Delta Wing with Half-Delta Tip Ailerons. NACA RM L9L14, 1950.

7. Seamans, Robert C., Jr., Bromberg, Benjamin G., and Payne, L. E.: Application of the Performance Operator to Aircraft Automatic Control. Jour. Aero. Sci., vol. 15, no. 9, Sept. 1948, pp. 535-555.

TABLE I

AIRFRAME PARAMETER VARIATIONS

Parameters Considered

Parameter	Variation	Reason for consideration
Mach Number	2.0 and 2.5	Expected flight conditions
Altitude, ft	20,000 and 40,000	
I_X, slug-ft^2	2.5 and 3	Estimated maximum and minimum values
$L_{\dot{\phi}}$	Estimated values and one-half estimated values	Effect of large overestimate on airframe characteristics

Values of Parameters Used in System Analyses

Flight condition	$L_{\dot{\phi}}$ (ft-lb/radian/sec)	I_X (slug-ft^2)	L_{δ_a} (ft-lb/radian)
M = 2 at 20,000 ft	-6.87	2.5	850
M = 2.5 at 40,000 ft	-2.99	3.0	377.5

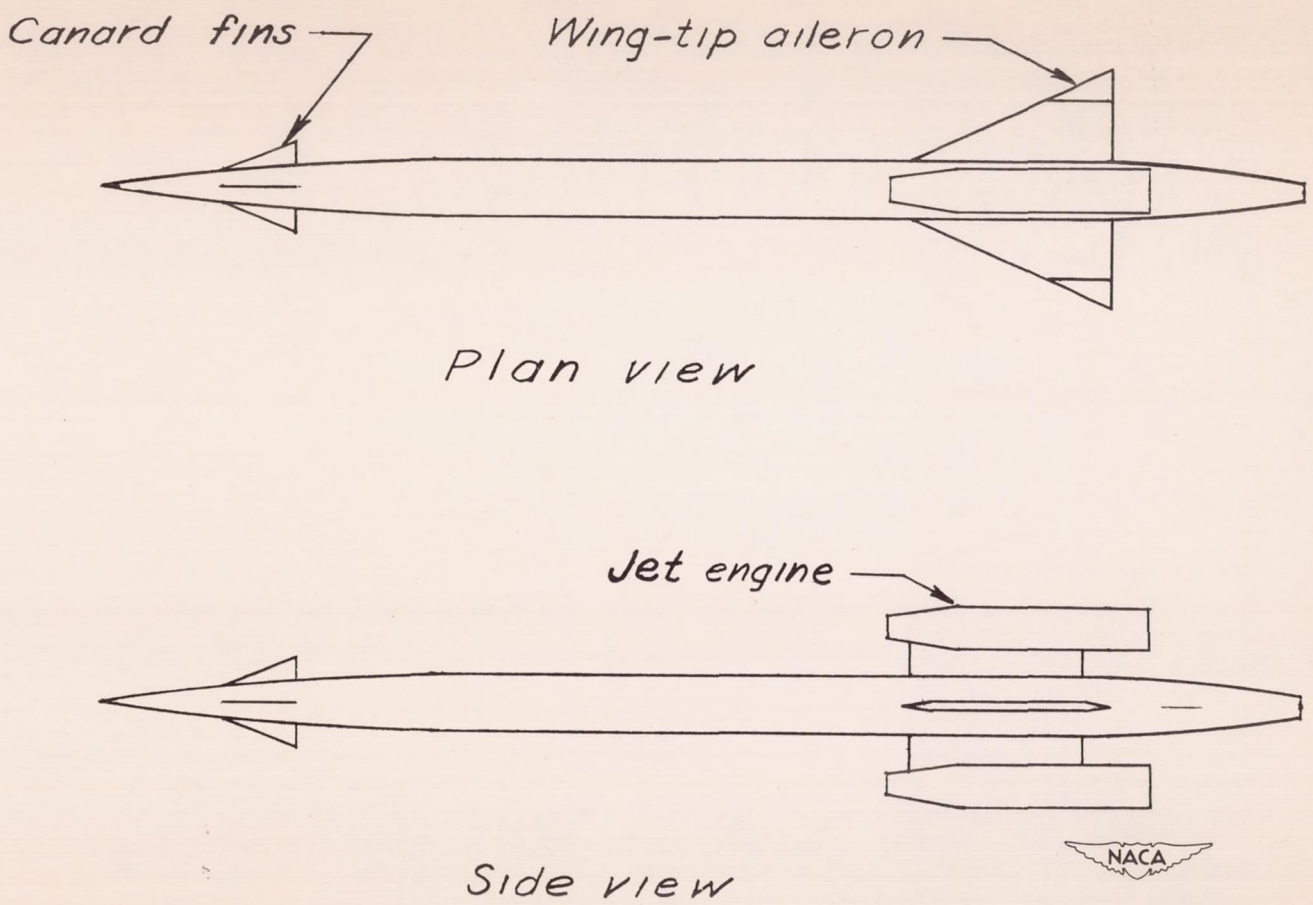

Figure 1.- Sketch of pilotless aircraft to be roll-stabilized.

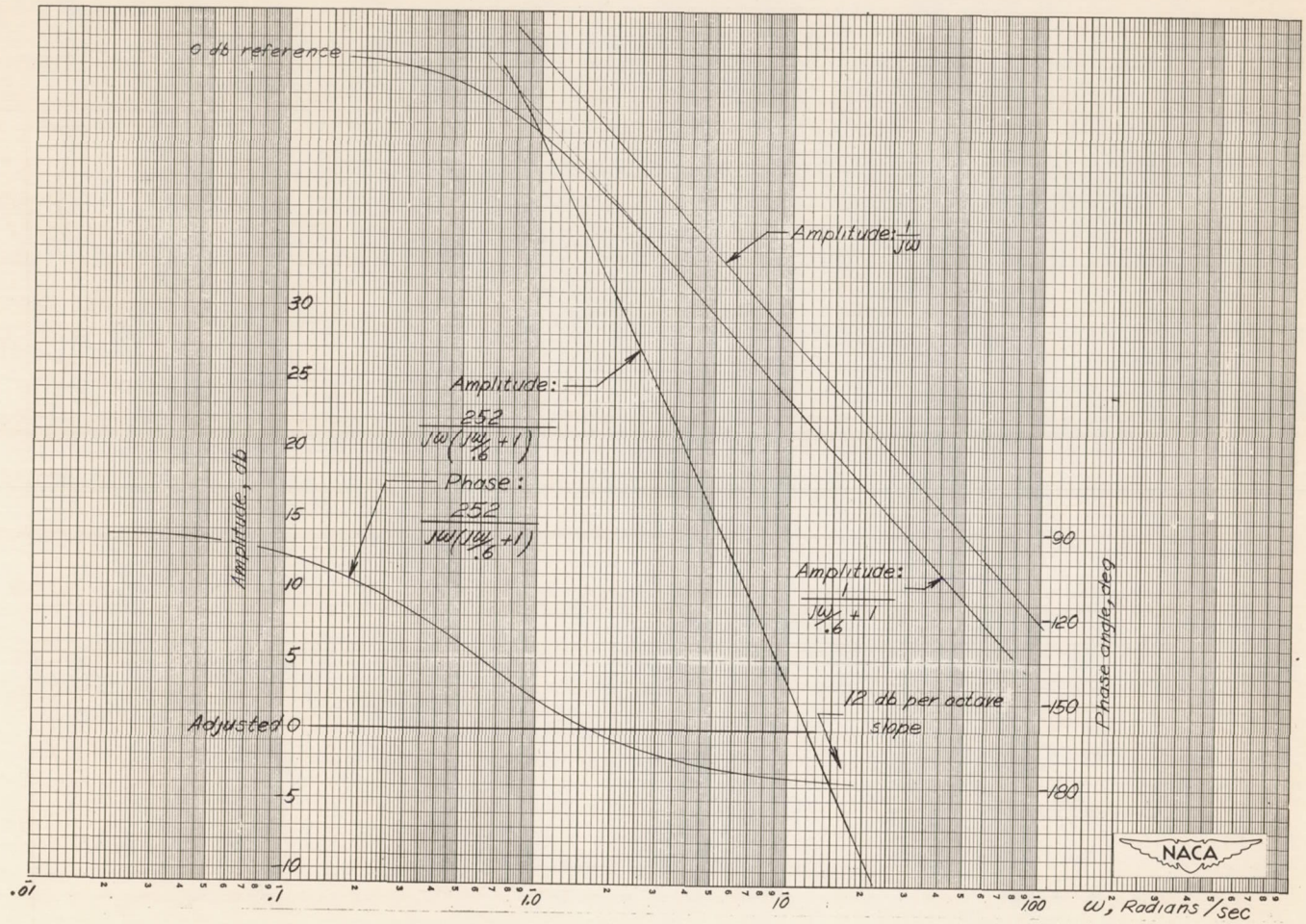

Figure 2.- Typical airframe ϕ/δ_a frequency response graphical construction on semilog graph paper. $\frac{L_{\delta_a}}{-L_{\dot{\phi}}} = 252$; $\frac{-L_{\dot{\phi}}}{I_X} = 0.6$; $I_X = 2.5$; M = 2.5; altitude, 40,000 feet; $L_{\dot{\phi}} = \frac{1}{12}$ estimated value.

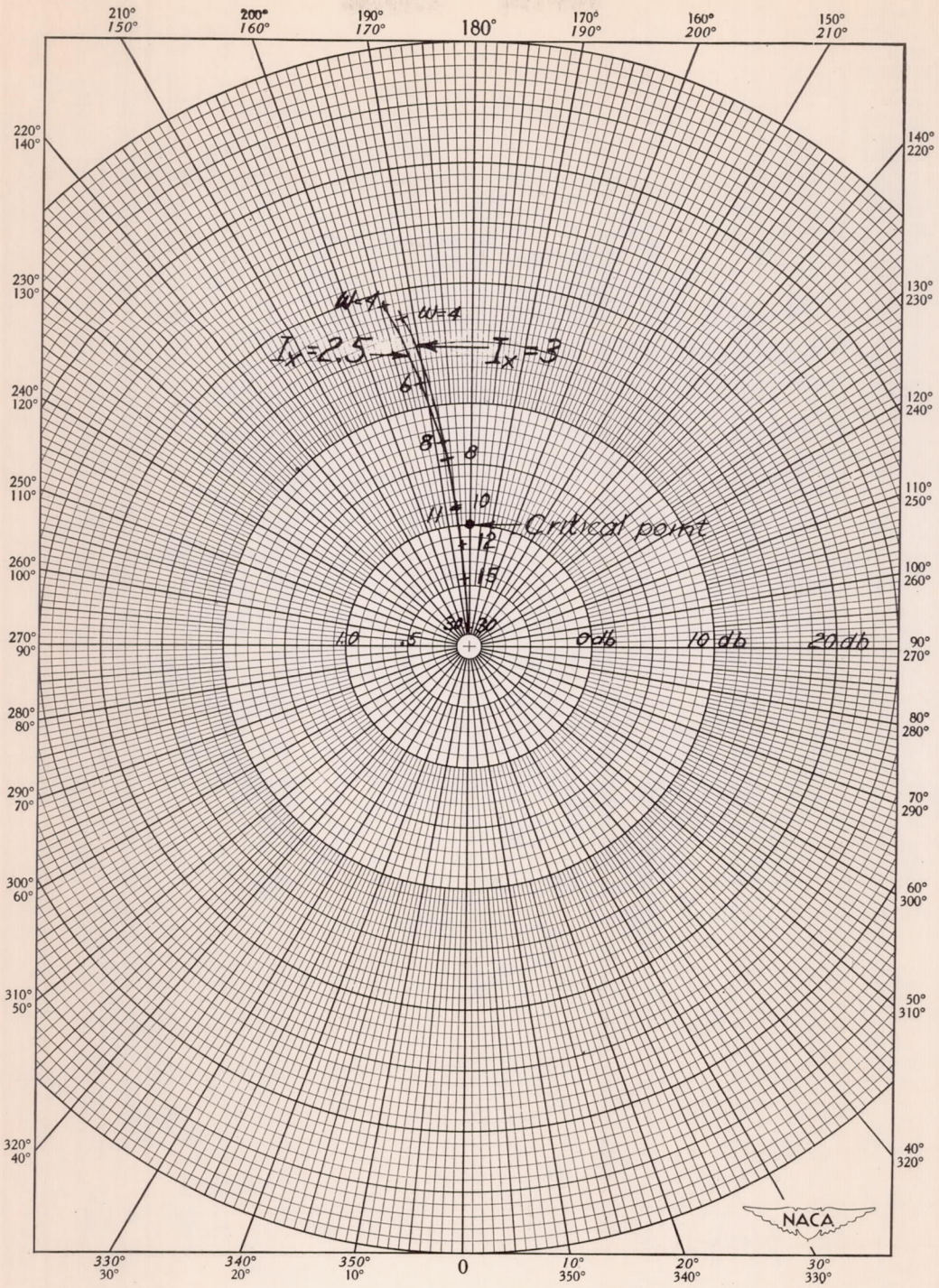

(a) Comparison of airframe ϕ/δ_a frequency responses for varying I_X. M = 2.5; altitude, 40,000 feet; estimated value of $L\dot{\phi}$.

Figure 3.- Nyquist diagrams of airframe frequency responses for inertia-, aerodynamic-, and flight-parameter changes.

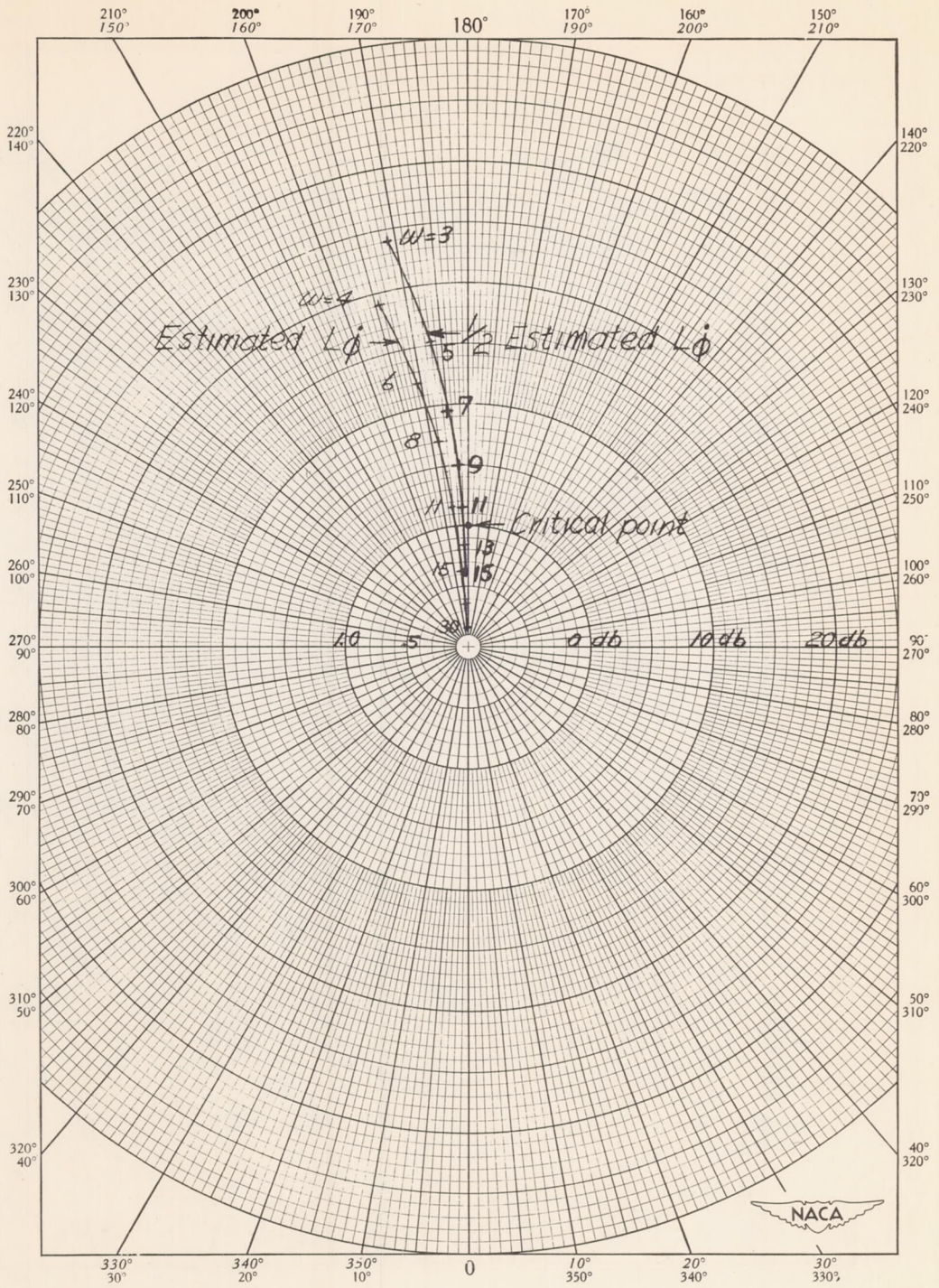

(b) Comparison of airframe ϕ/δ_a frequency responses for varying aerodynamic damping. M = 2.5; altitude, 40,000 feet; I_X = 2.5.

Figure 3.- Continued.

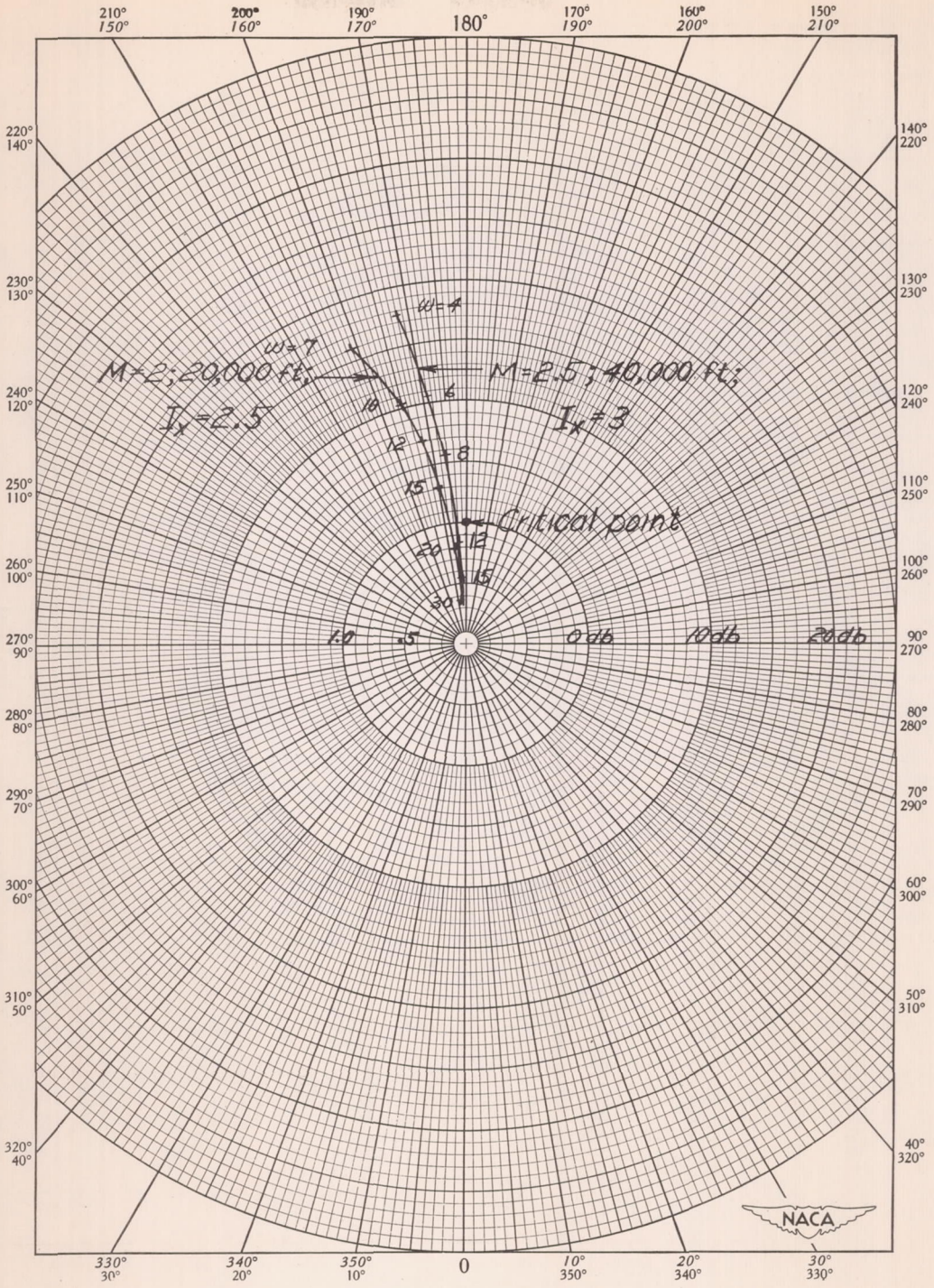

(c) Airframe frequency responses for the two extreme conditions chosen for automatic stabilization analyses using estimated values of $L\dot{\phi}$.

Figure 3.- Concluded.

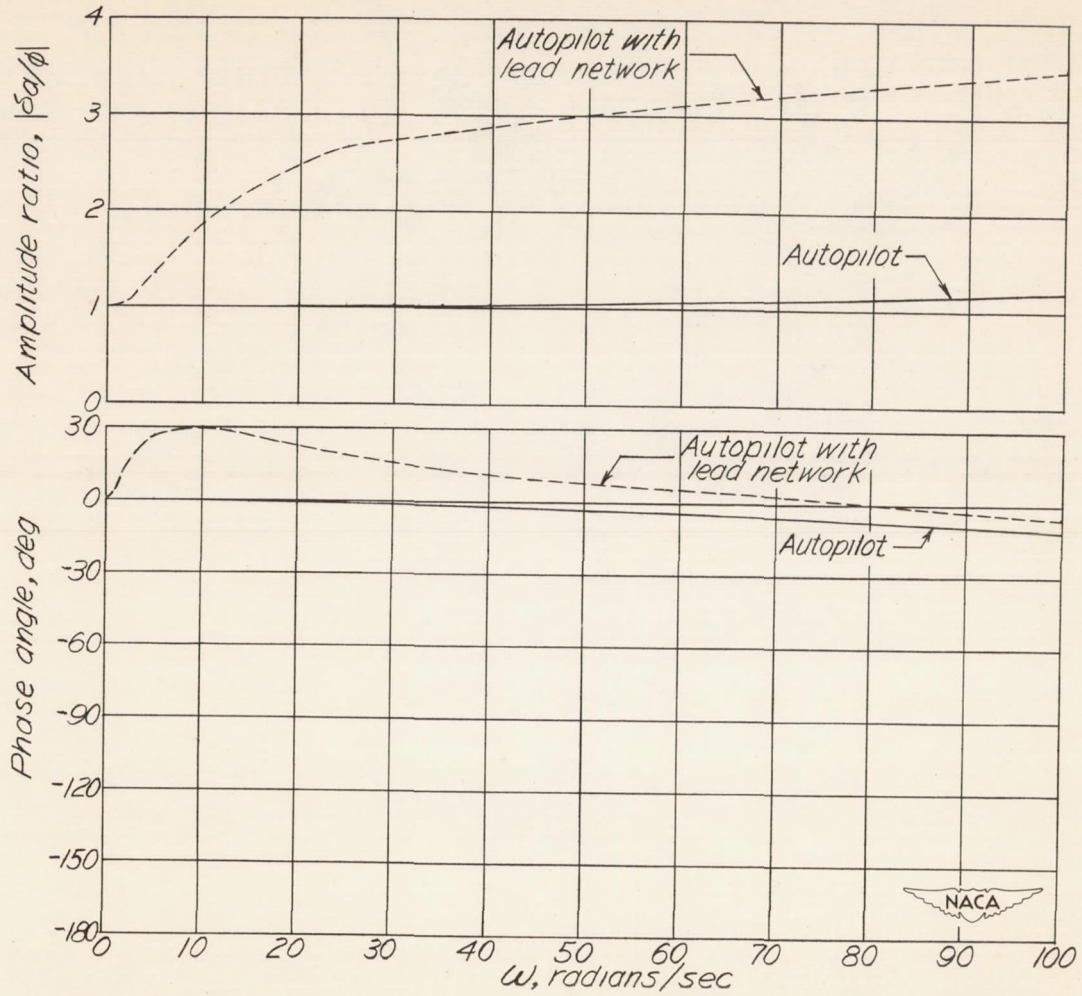

Figure 4.- Experimentally determined δ_a/ϕ frequency response of the electronic-hydraulic autopilot and the calculated effect of a lead network in cascade with the autopilot on the δ_a/ϕ frequency response. Static ($\omega = 0$) gain adjusted to unity.

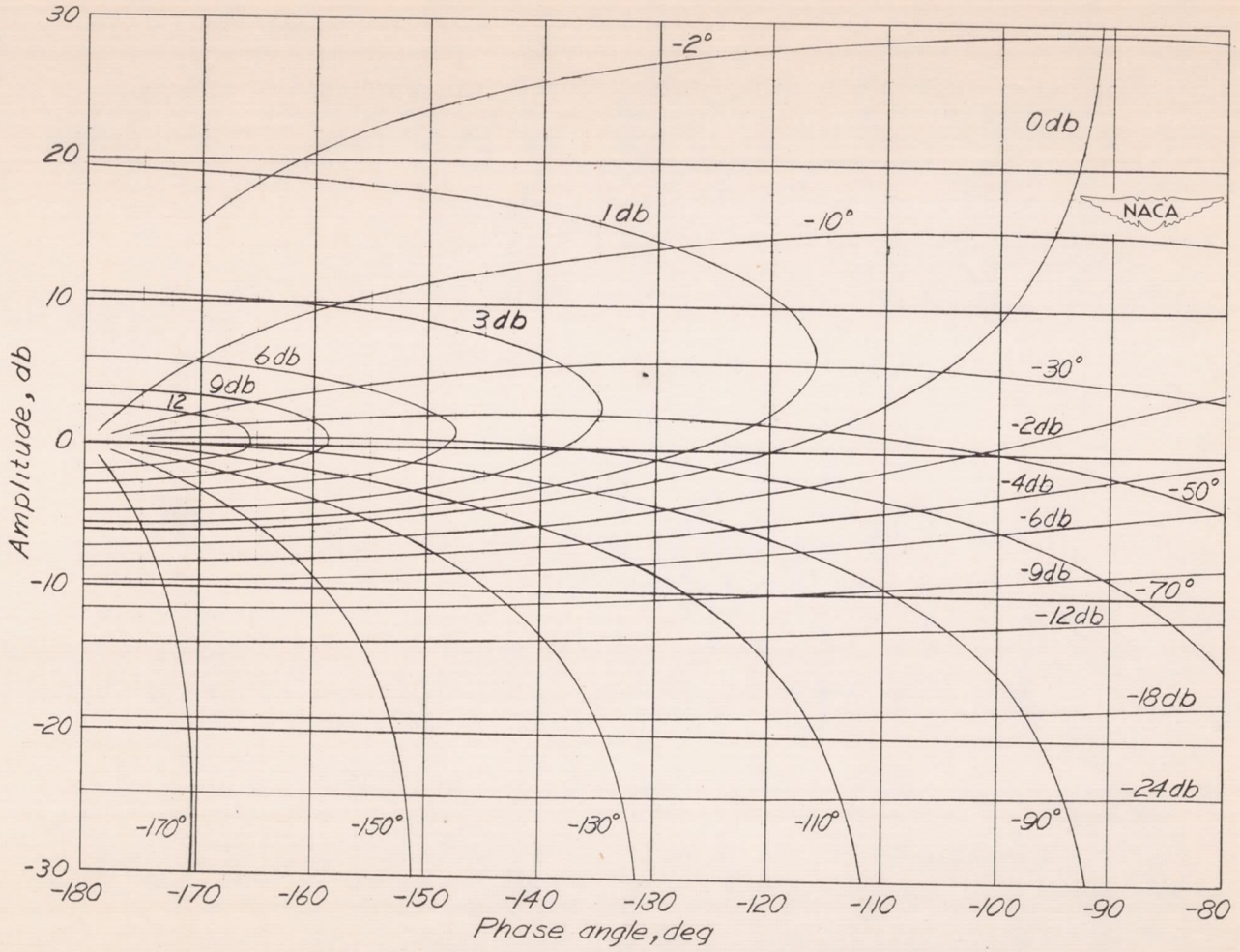

Figure 5.- Reproduction of M-N contour chart showing open-loop values on rectangular coordinates and closed-loop values on curved coordinates.

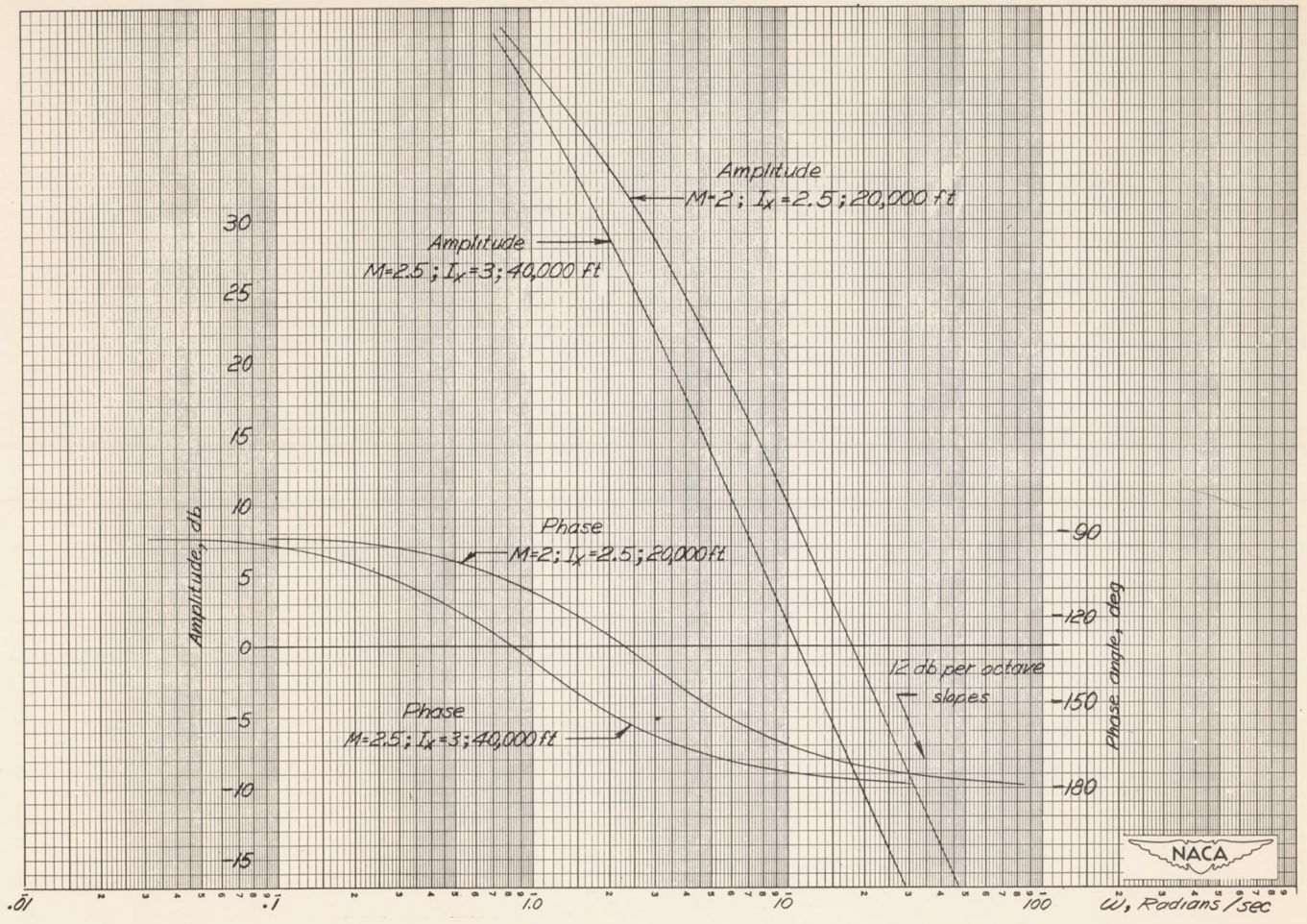

(a) ϕ/δ_a airframe frequency responses constructed graphically on semilog graph paper for the assumed extreme conditions of flight.

Figure 6.- Series of graphs used to analyze the characteristics of the airframe and gyro-actuated-control roll-stabilization system.

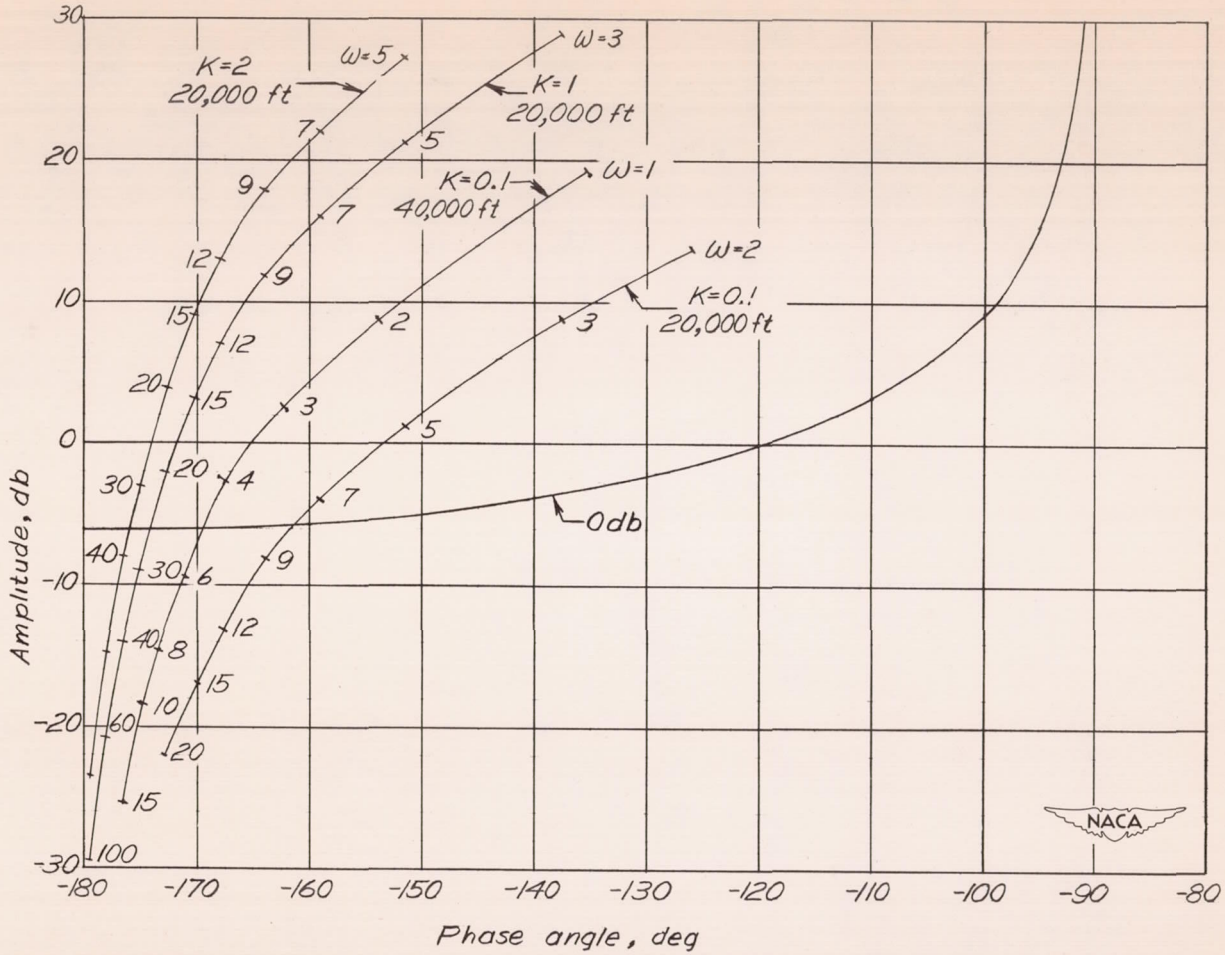

(b) Plots of system open-loop frequency responses for three values of K (gain adjustment) on M-N contour chart. Closed-loop contours (other than 0 db) omitted for simplicity.

Figure 6.- Continued.

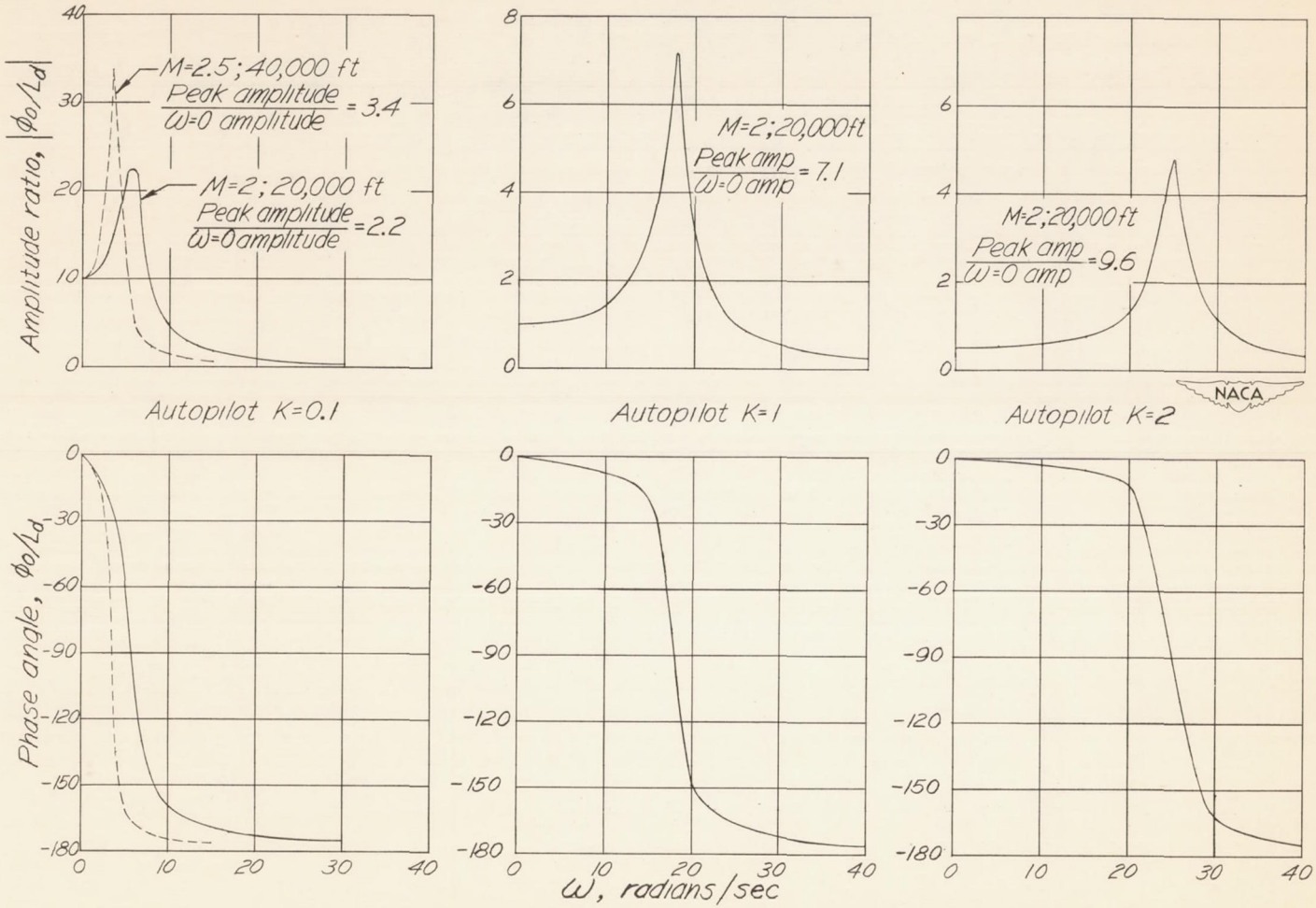

(c) Closed-loop ϕ_o/L_d frequency responses corresponding to the open-loop frequency-response curves of figure 6(b).

Figure 6.- Concluded.

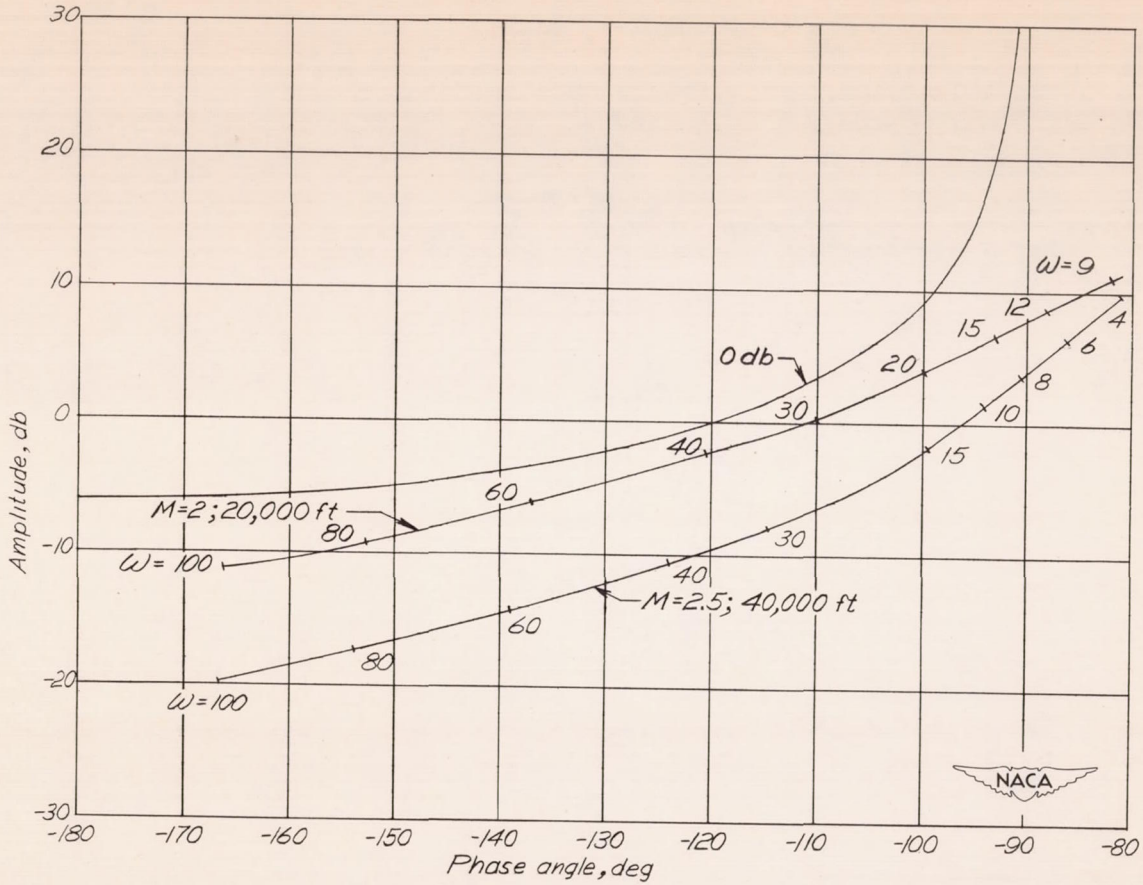

(a) Plots of inner-loop open-loop frequency responses on M-N contour chart. Closed-loop contours (other than 0 db) omitted.

Figure 7.- Series of graphs used to analyze the airframe, rate gyro-pneumatic servo and gyro-actuated-control composite roll stabilization system. Rate servo static sensitivity $K_r = 0.1$. Gyro-actuated control adjusted gain $K = 2.1$.

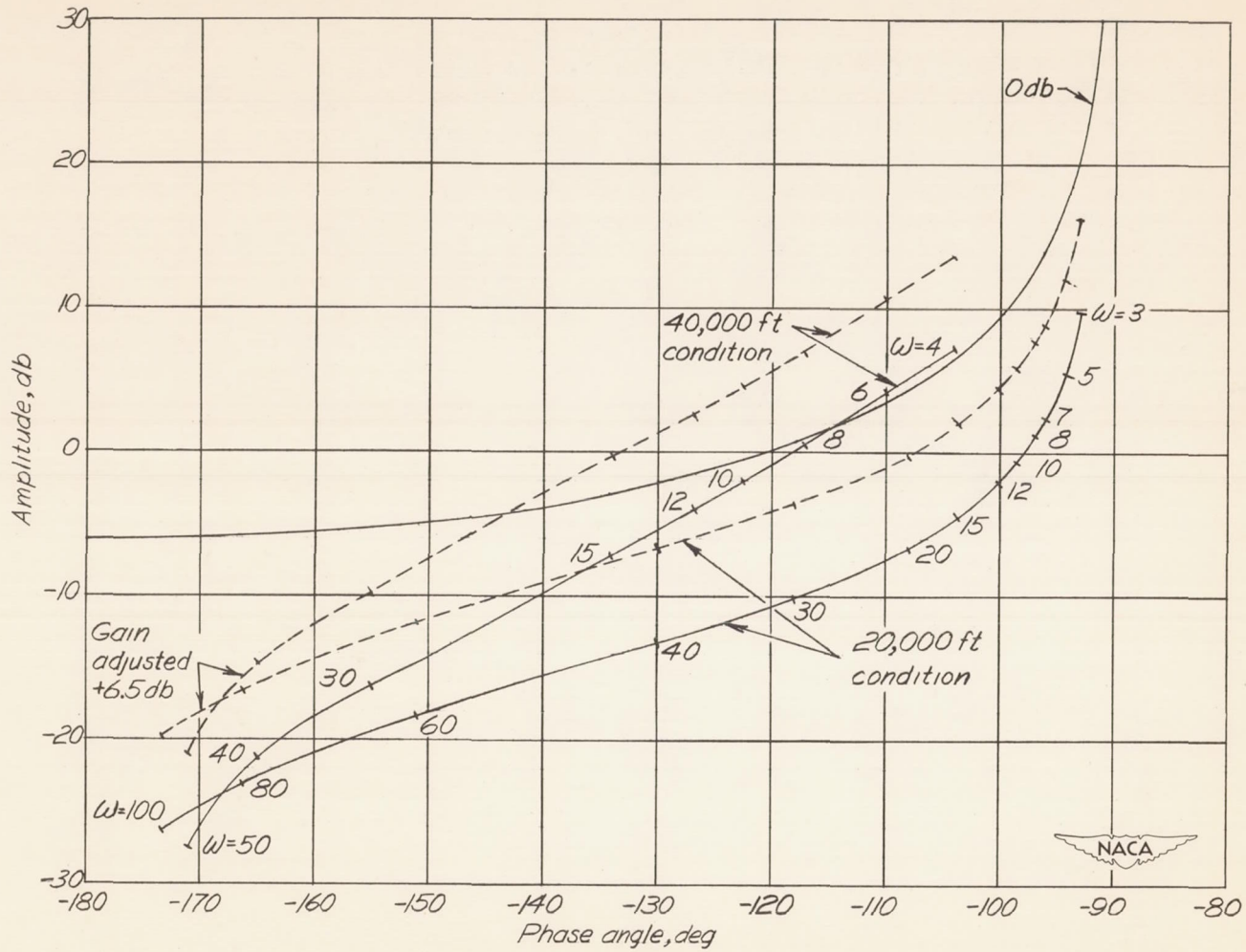

(b) System open-loop frequency responses on M-N contour chart. Closed-loop contours (other than 0 db) omitted.

Figure 7.- Continued.

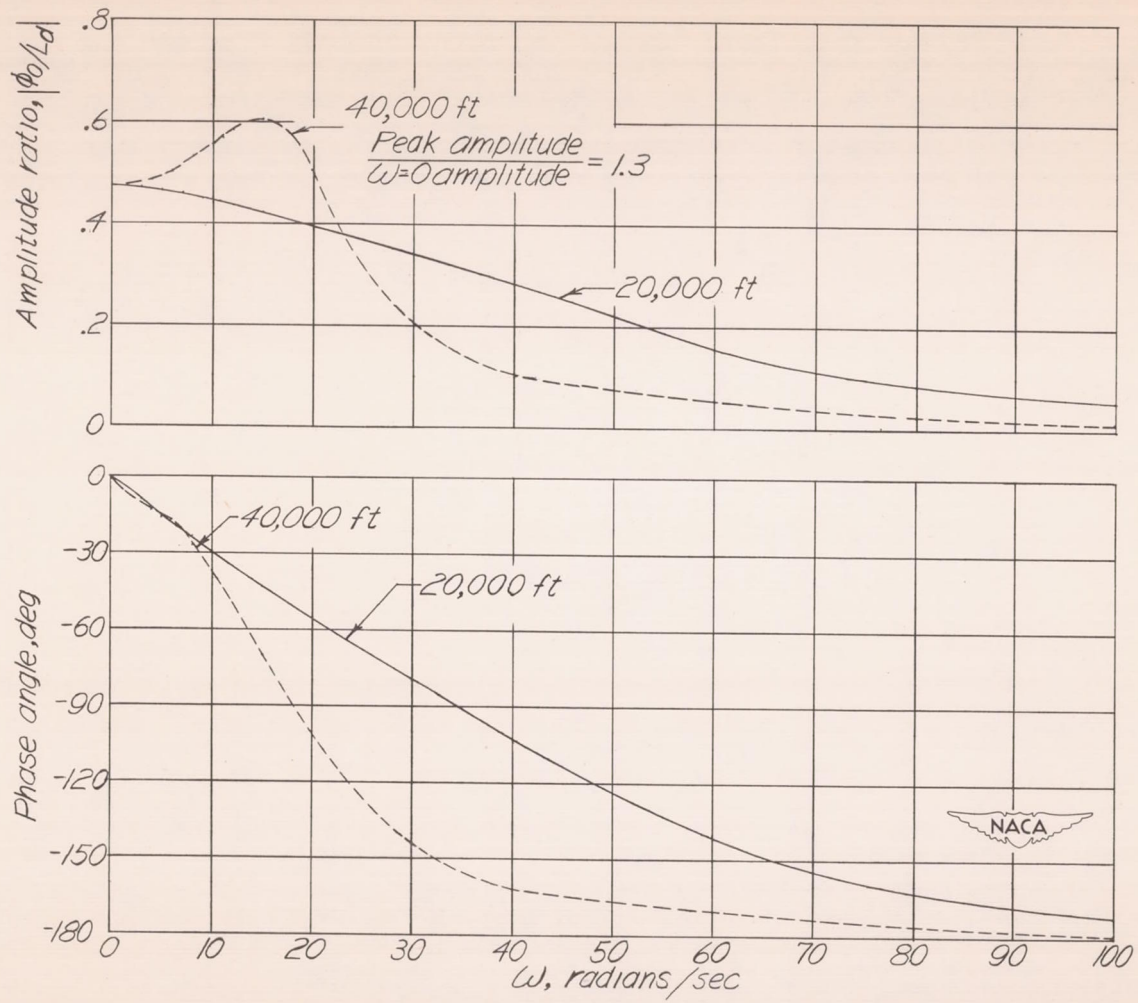

(c) System closed-loop frequency responses, $\phi_o/L_d(j\omega)$, for the assumed extreme flight conditions.

Figure 7.- Concluded.

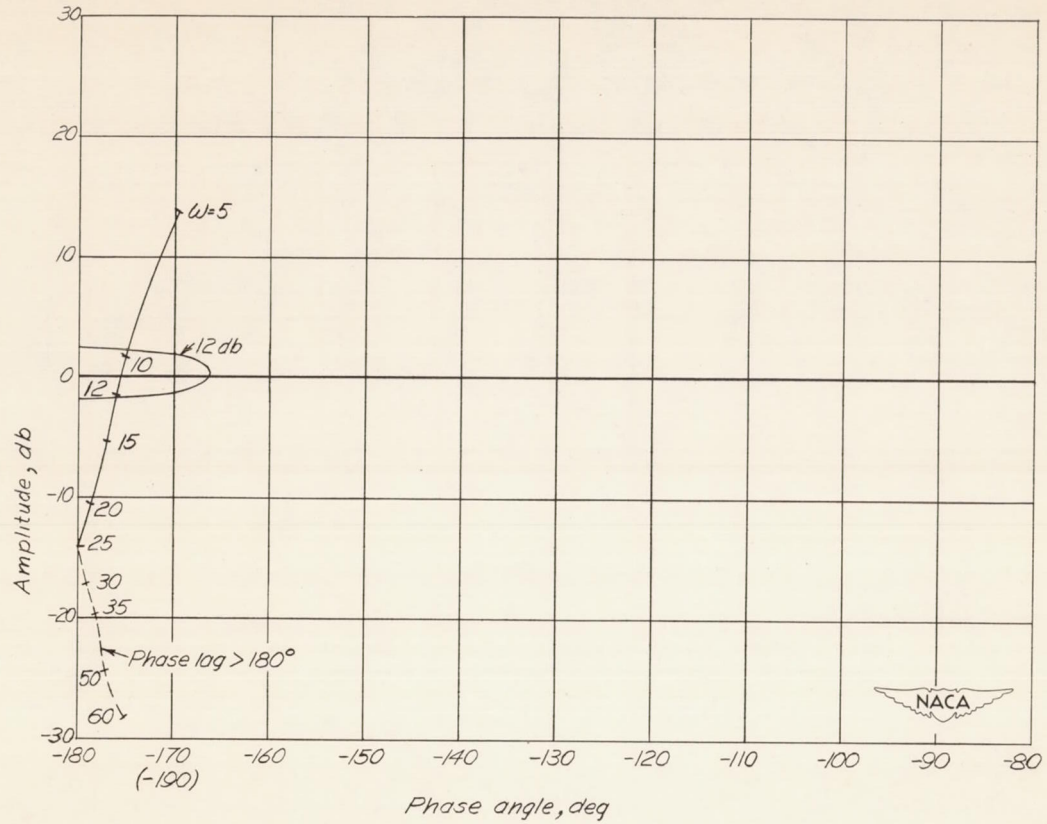

(a) Open-loop frequency response plotted on M-N contour chart. Closed-loop contours (other than 12 db) omitted.

Figure 8.- Frequency responses for the system composed of the airframe and electronic-hydraulic autopilot without corrective networks. 40,000-foot-altitude flight condition; no gain adjustment (autopilot $\frac{\delta_a}{\phi} = 1$).

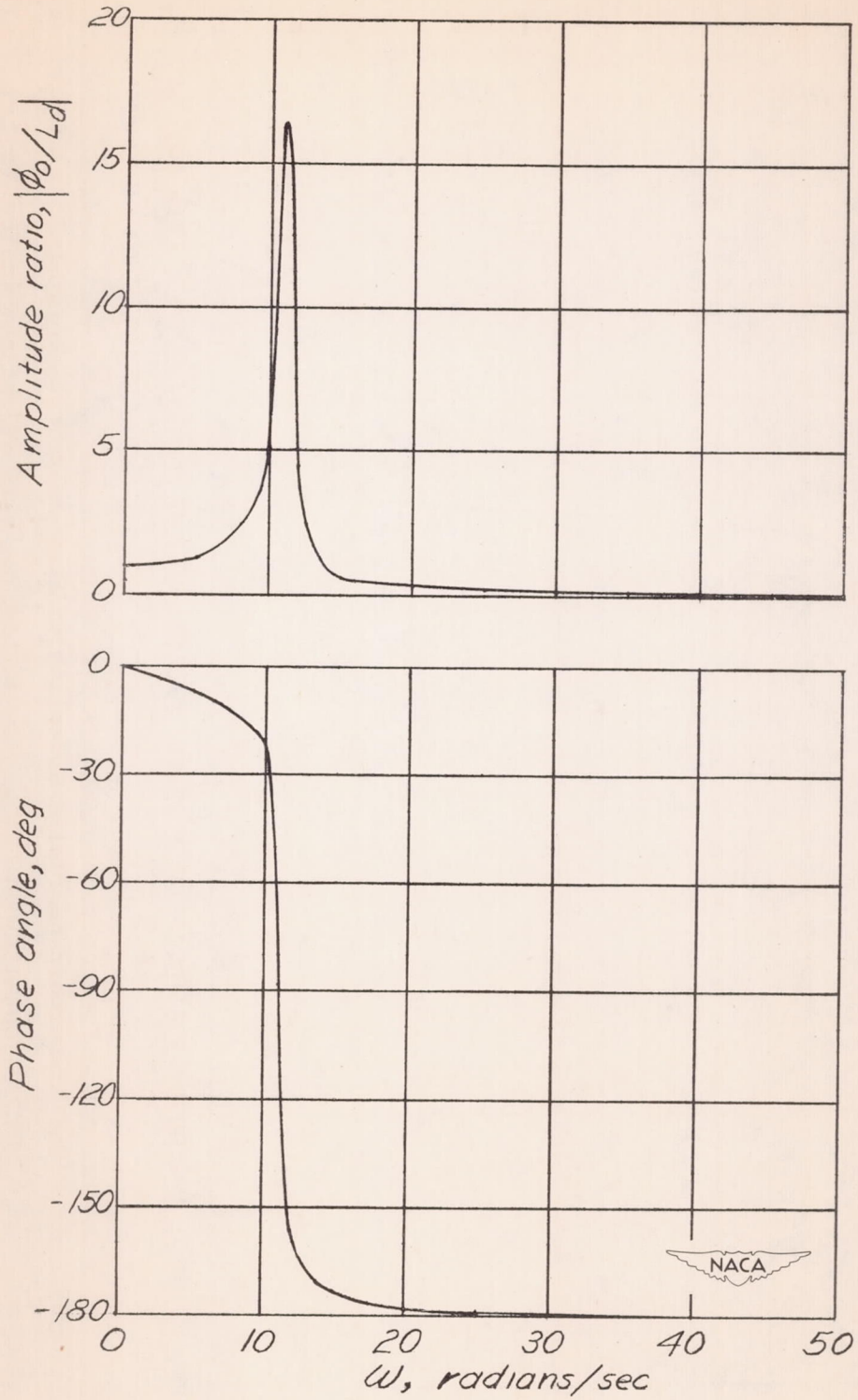

(b) System closed-loop frequency response.

Figure 8.- Concluded.

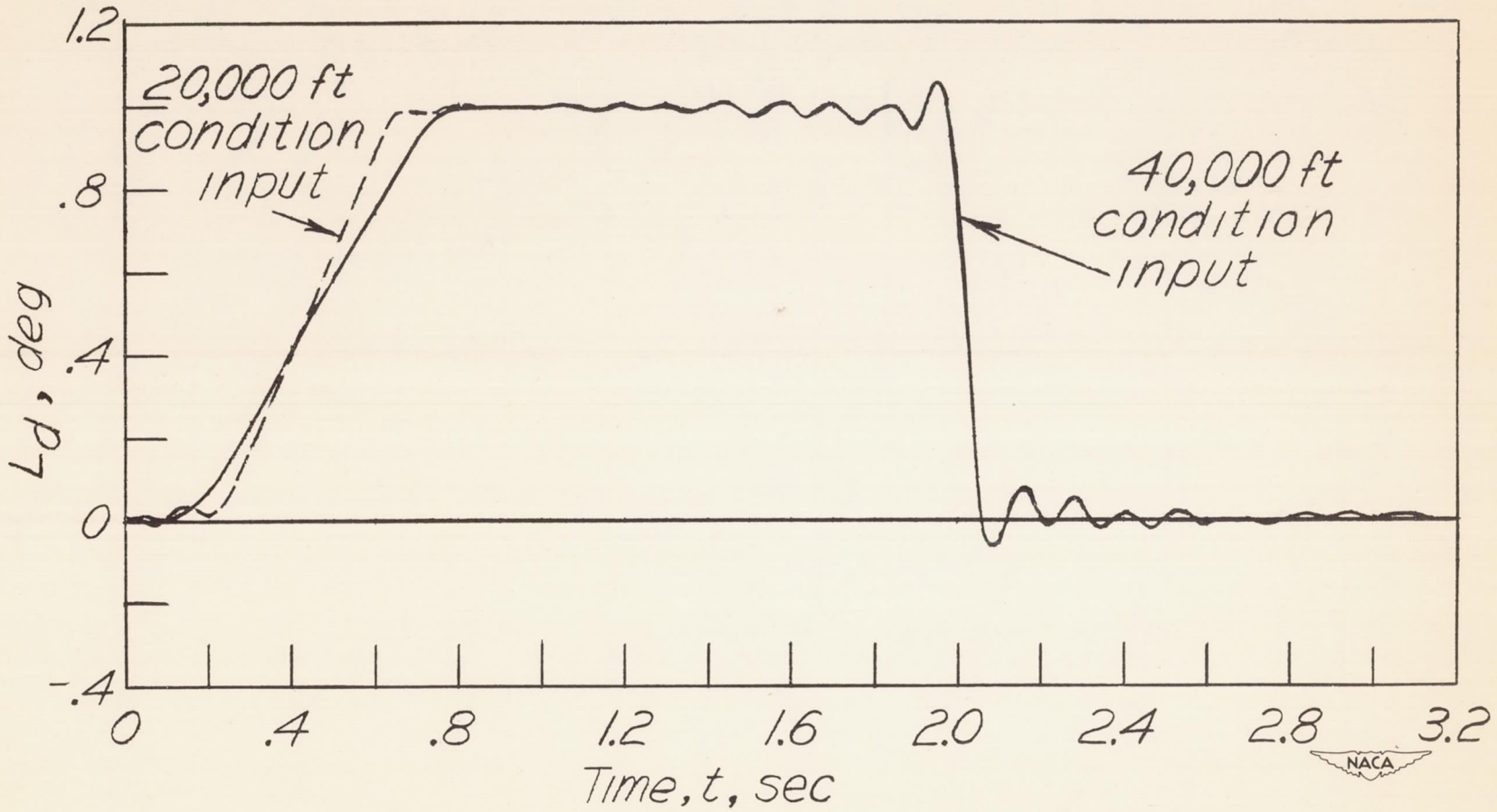

Figure 9.- Complete cycle of ramp input summation curves for the assumed extreme flight conditions as determined from the Fourier synthesizer. Zero time arbitrarily chosen during the cycle. Input period, 3.14 seconds.

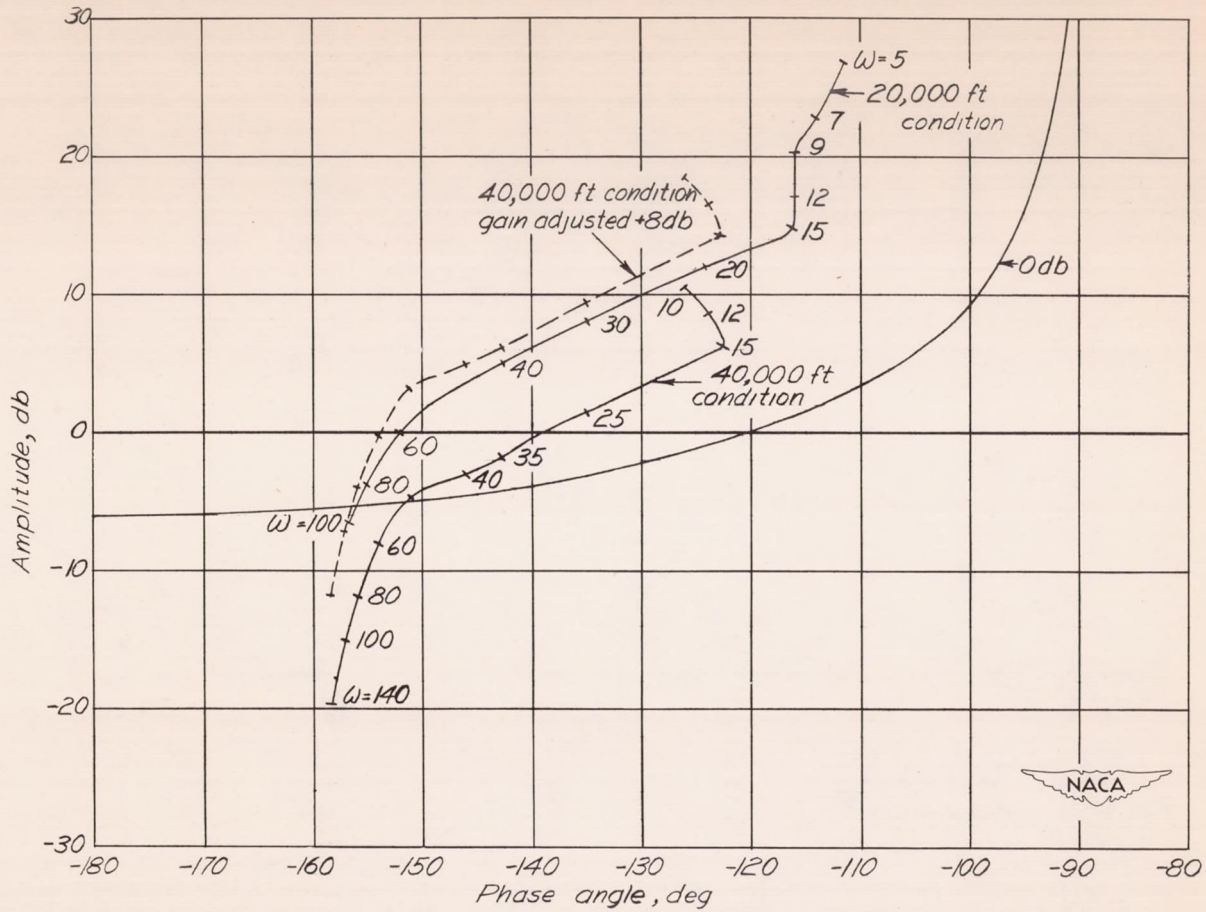

(a) Open-loop frequency response on M-N contour chart. Closed-loop contours (other than 0 db) omitted.

Figure 10.- Frequency responses of the airframe and electronic-hydraulic autopilot with a lead network. Lead network and autopilot combined frequency response experimentally determined.

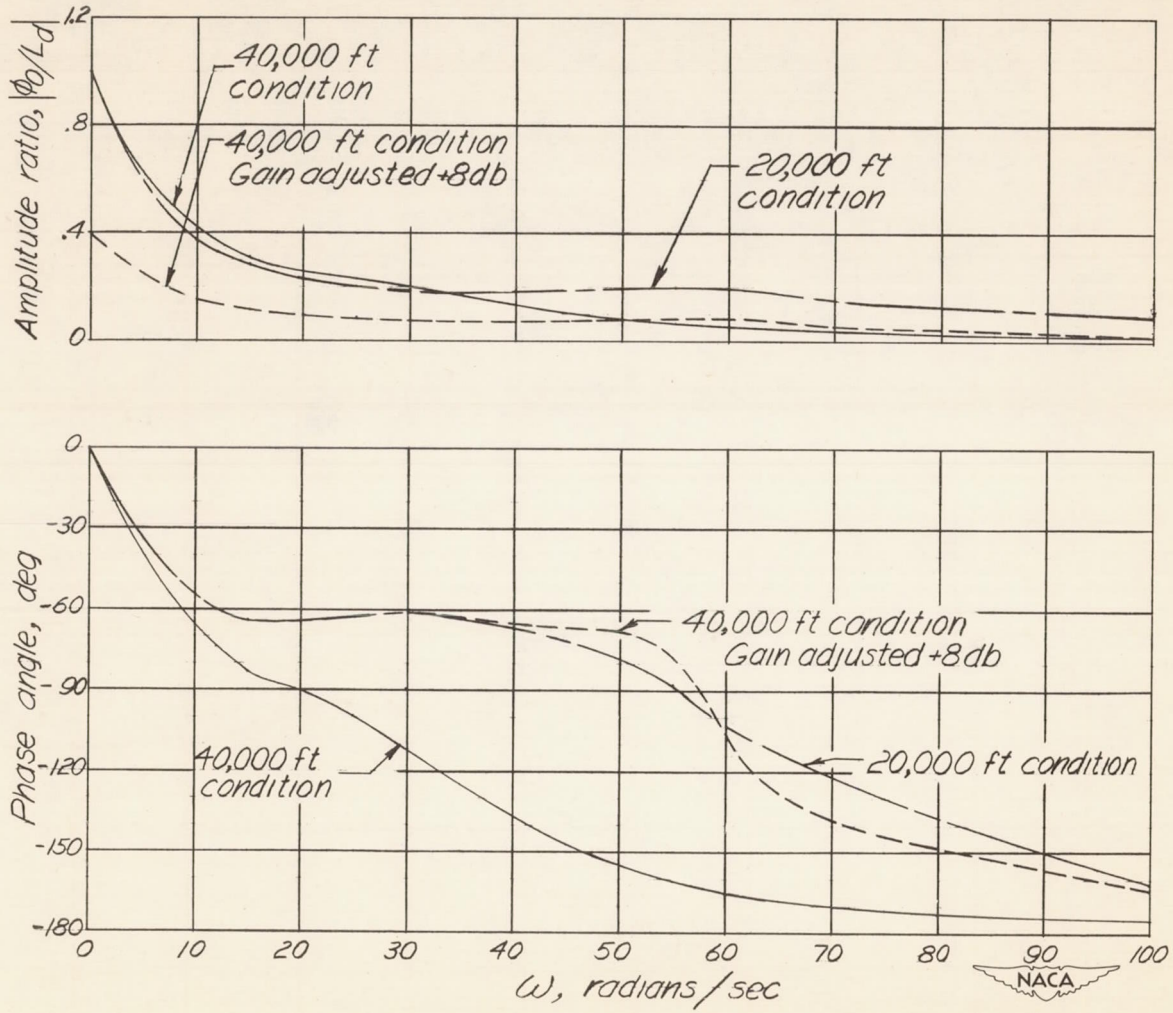

(b) Closed-loop system frequency responses, $\phi_o/L_d(j\omega)$.

Figure 10.- Concluded.

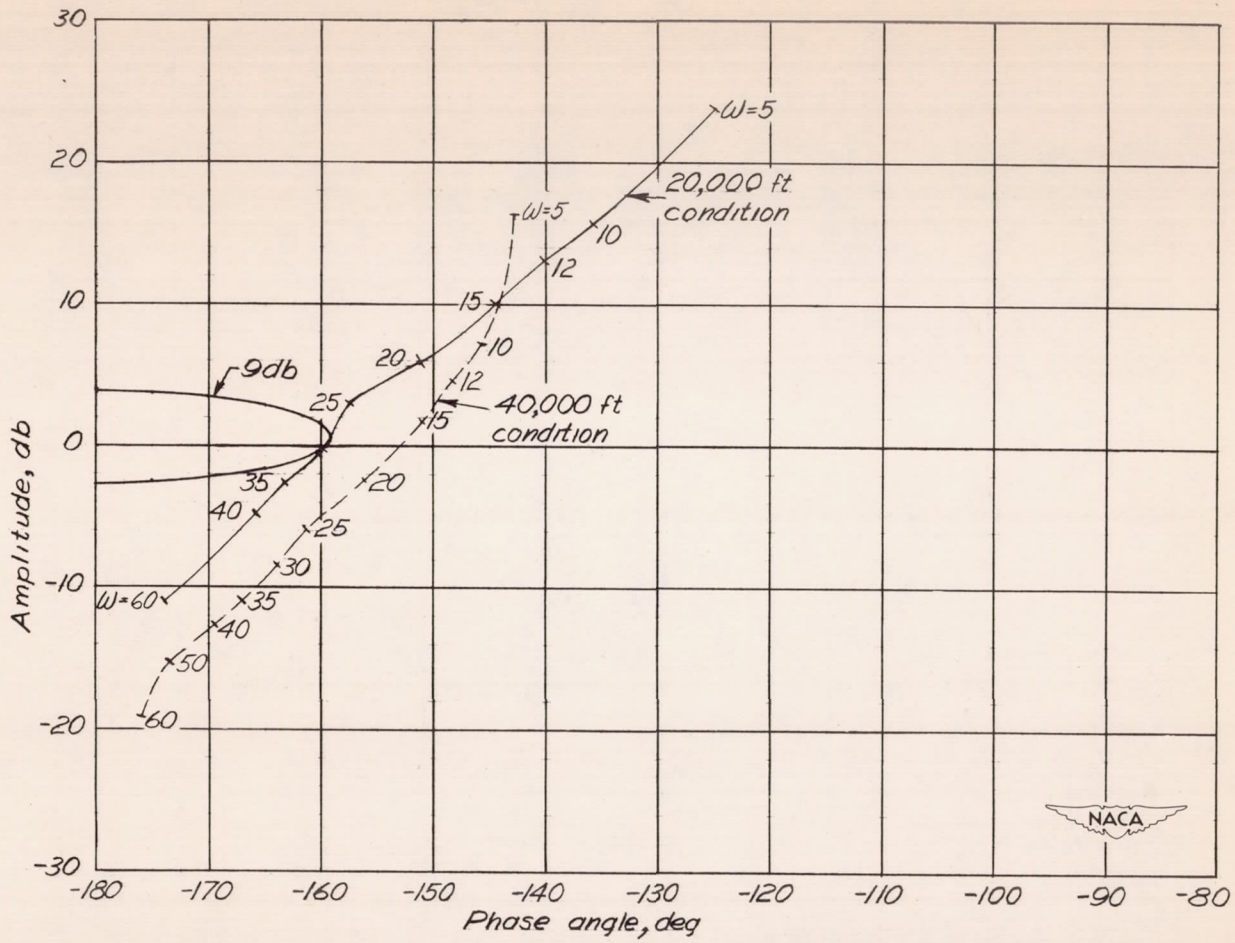

(a) Open-loop frequency responses on M-N contour chart. Closed-loop contours (other than 9 db) omitted.

Figure 11.- Responses of the system including the airframe and the electronic-hydraulic autopilot with $\alpha = 3$, $\omega_1 = 5$ lead network.

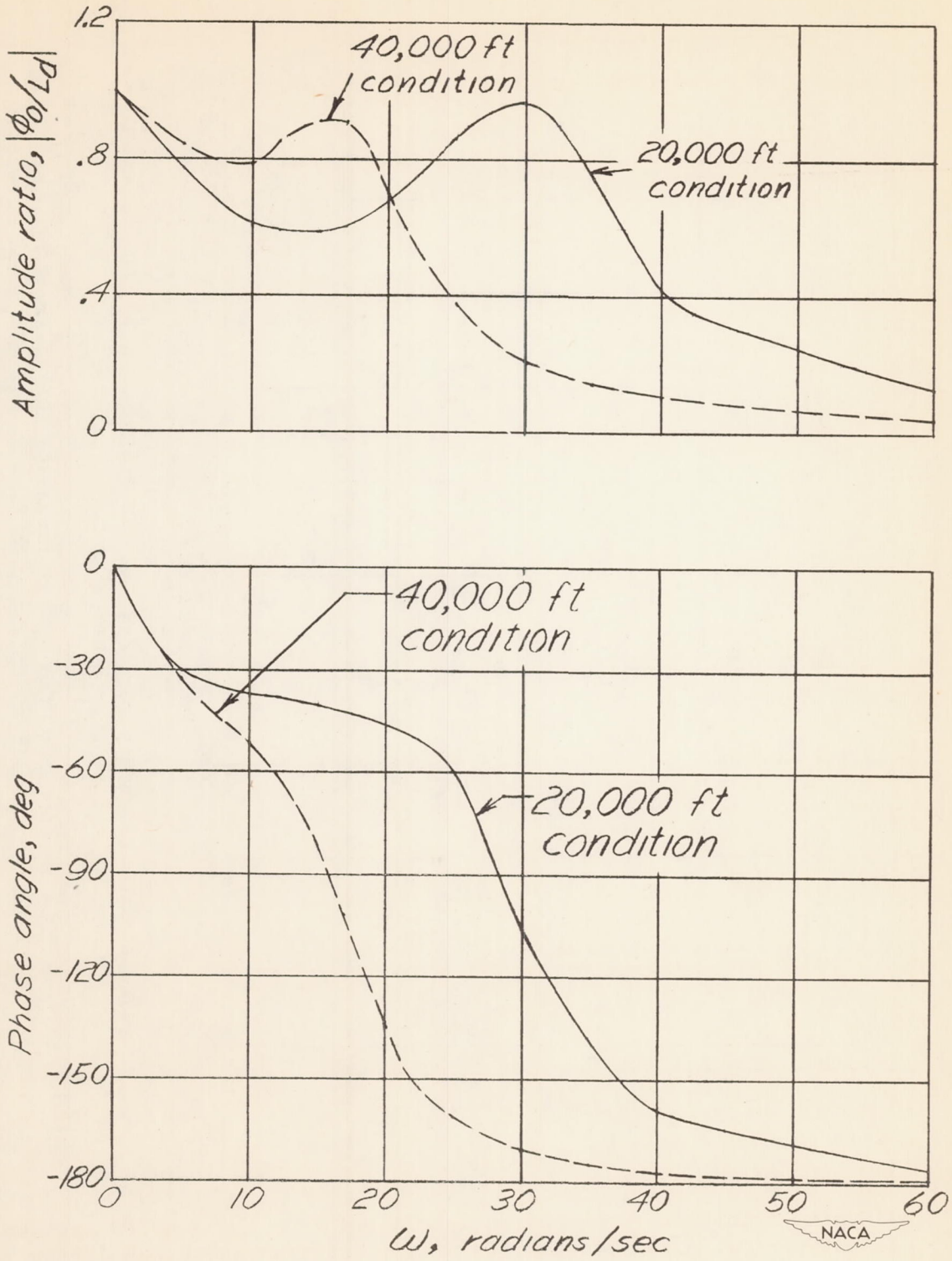

(b) System closed-loop frequency responses, $\phi_o/L_d(j\omega)$.

Figure 11.- Continued.

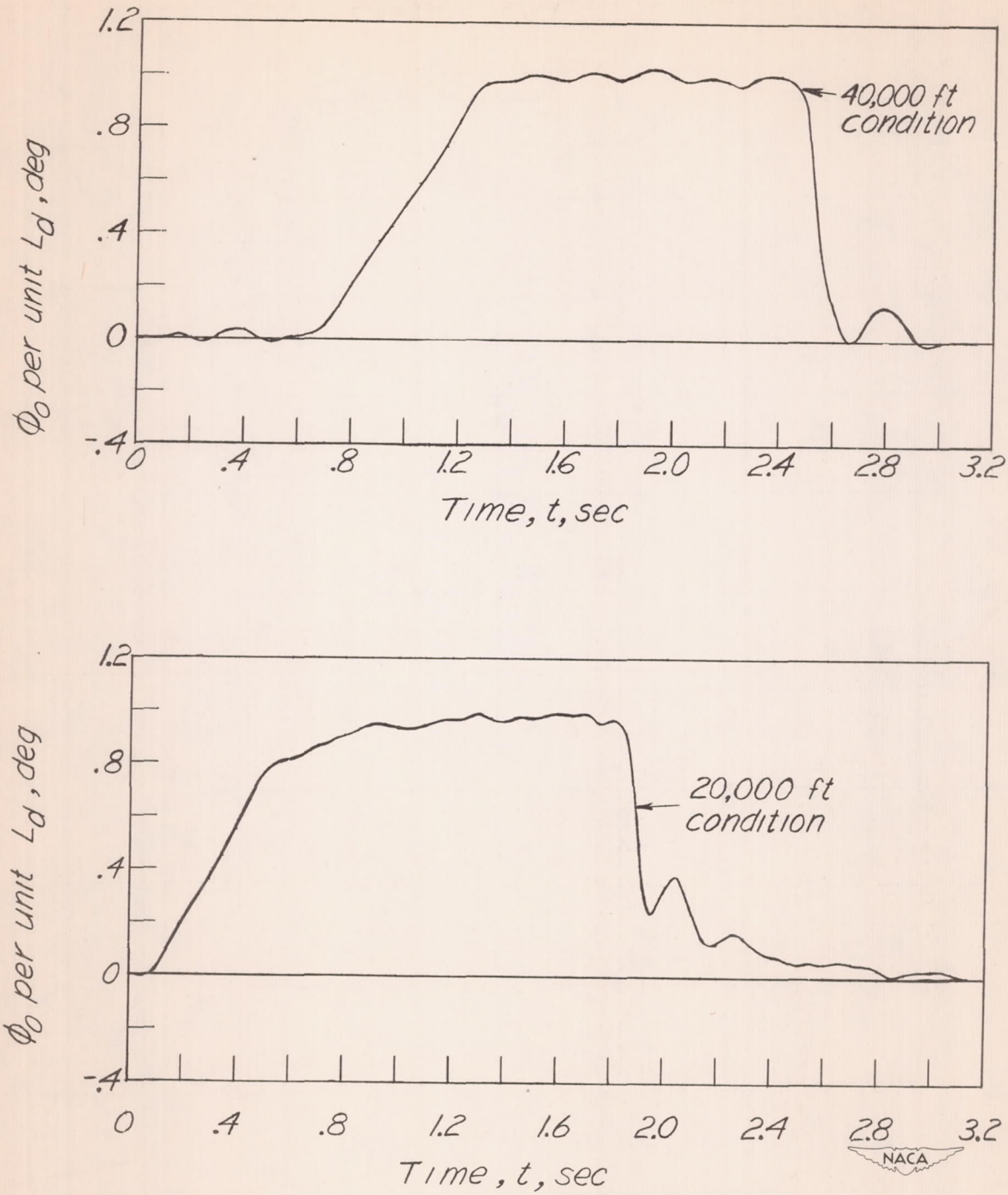

(c) System transient responses as determined from the Fourier synthesizer. Input period, 3.14 seconds. Zero time arbitrarily chosen during the cycle.

Figure 11.- Concluded.

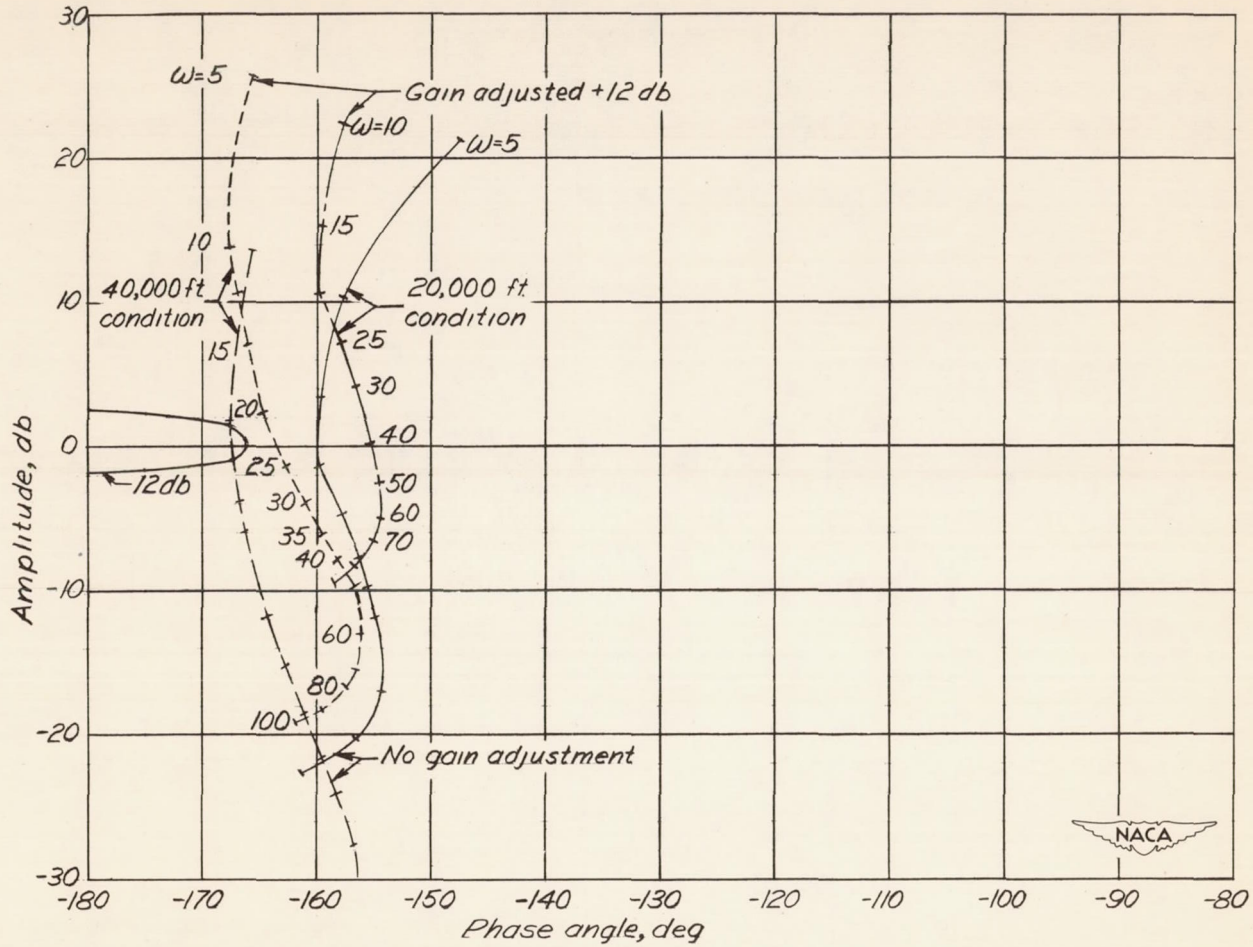

(a) Open-loop frequency responses on M-N contour chart. Closed-loop contours (other than 12 db) omitted.

Figure 12.- Responses of the system including the airframe and electronic-hydraulic autopilot with $\alpha = 3$, $\omega_1 = 50$ lead network.

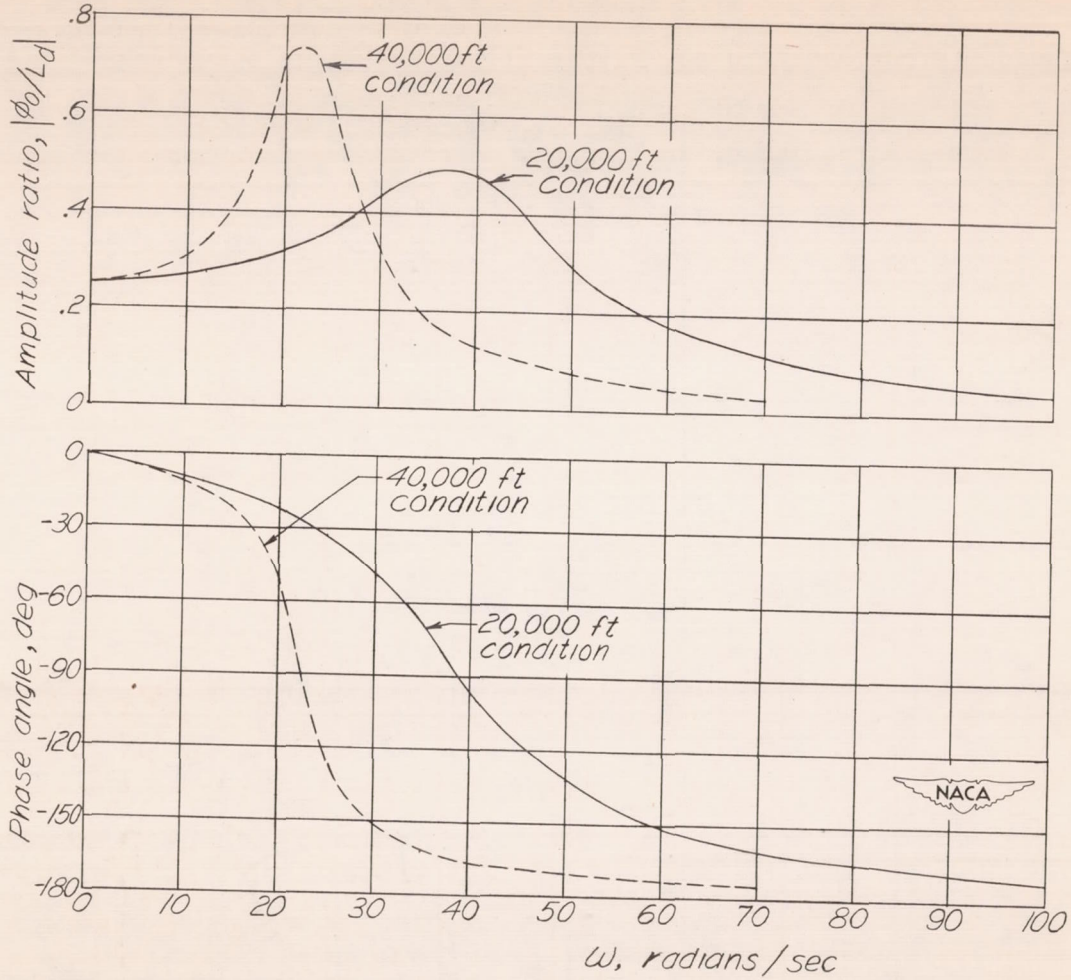

(b) Closed-loop frequency responses, $\phi_o/L_d(j\omega)$. Gain adjusted 12 decibels.

Figure 12.- Concluded.

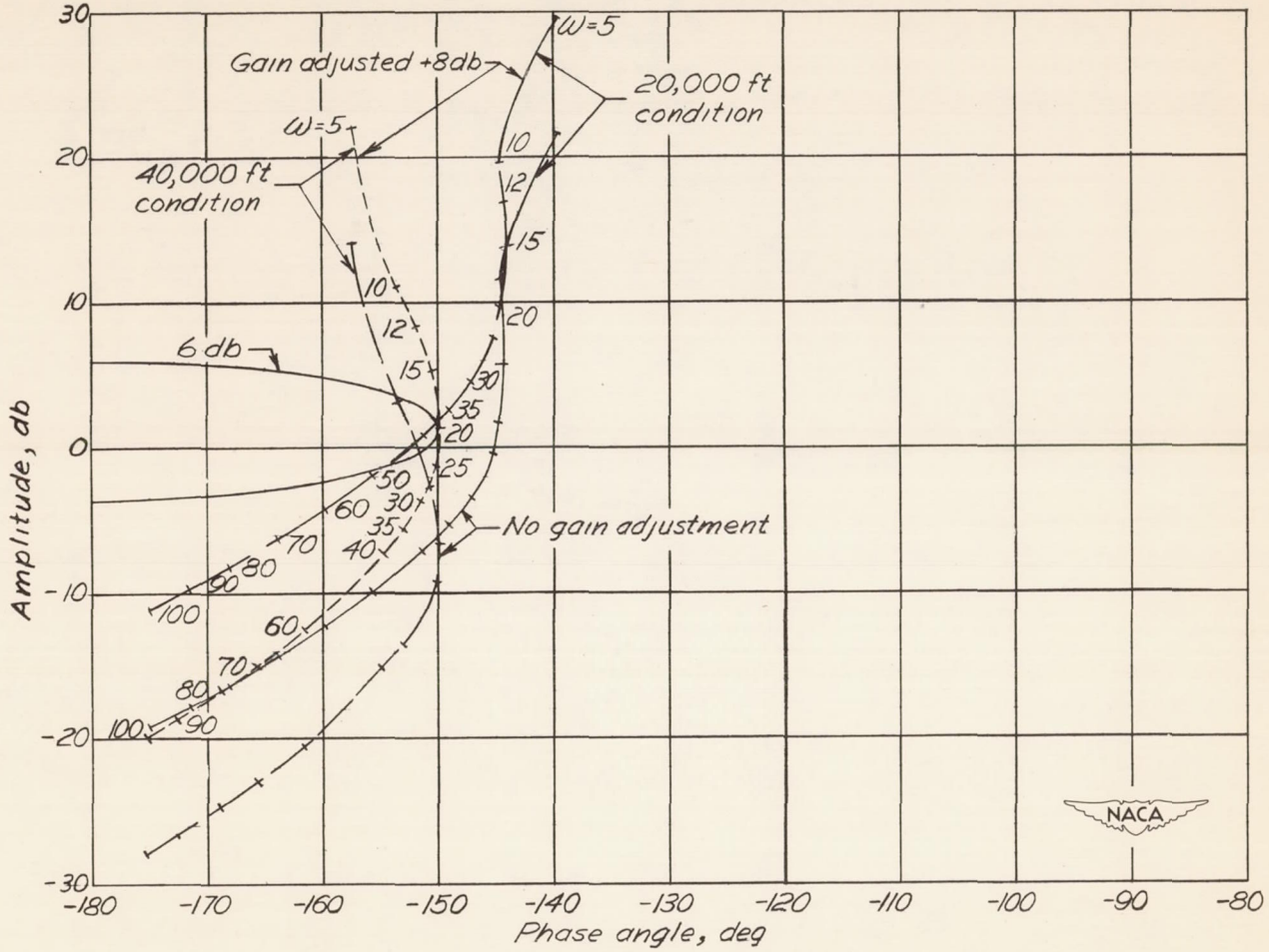

(a) System open-loop frequency responses on M-N contour chart. Closed-loop contours (other than 6 db) omitted.

Figure 13.- Responses of the system including the airframe and electronic-hydraulic autopilot with $\alpha = 3$, $\omega_1 = 15$ lead network.

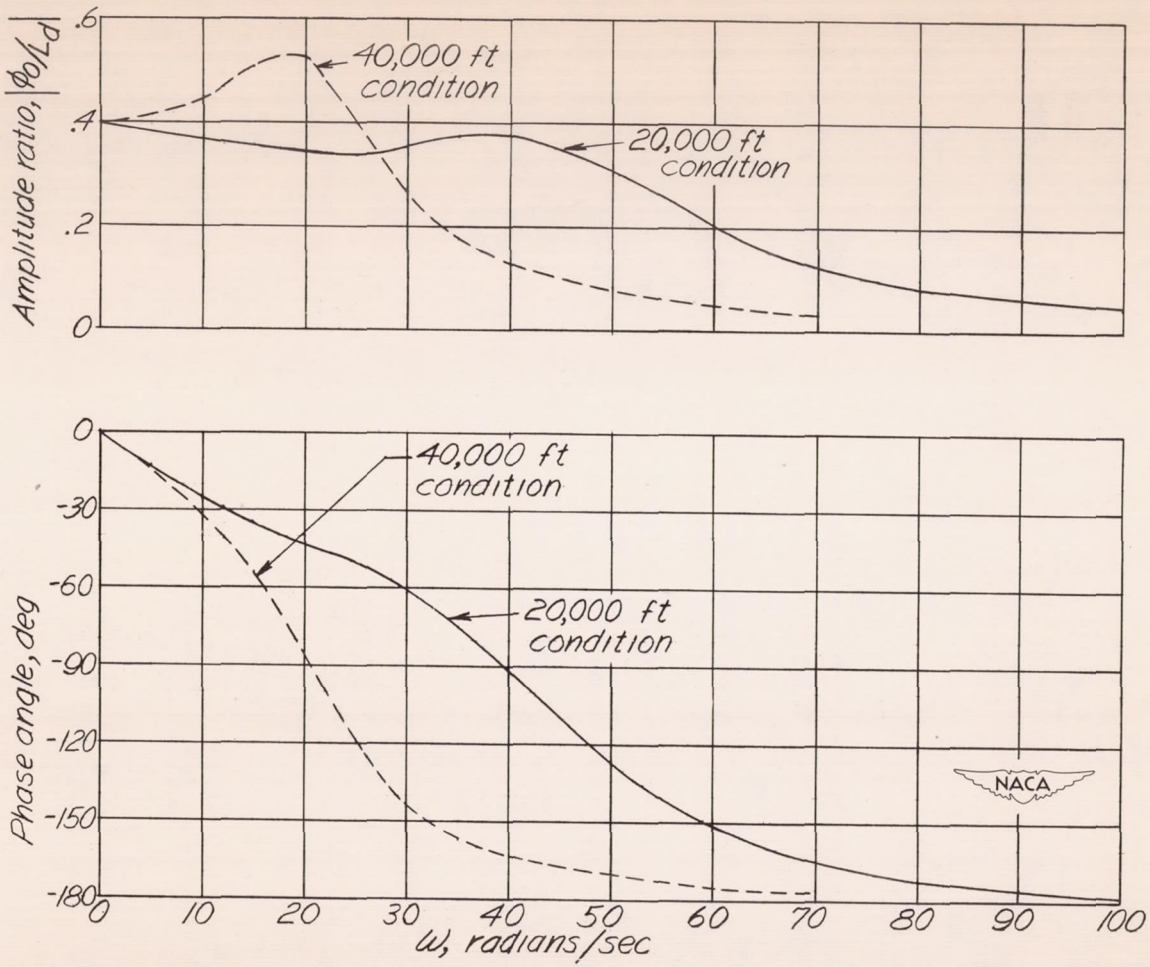

(b) Closed-loop frequency responses, $\phi_o/L_d(j\omega)$. Gain adjusted 8 decibels.

Figure 13.- Concluded.

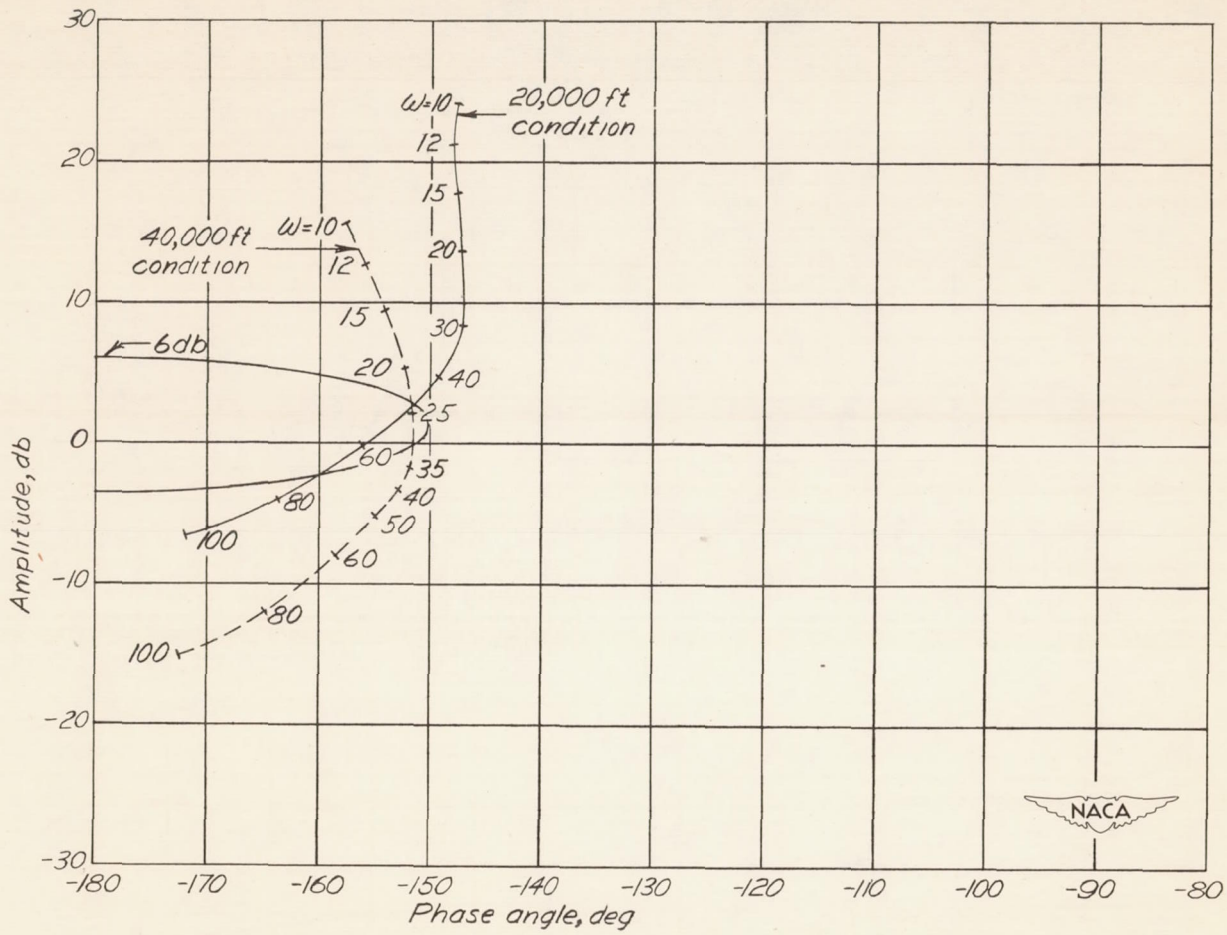

(a) System open-loop frequency responses on M-N contour chart. Closed-loop contours (other than 6 db) omitted.

Figure 14.- Responses of the system including the airframe and electronic-hydraulic autopilot with $\alpha = 3$, $\omega_1 = 20$ lead network. Gain adjusted 13 decibels.

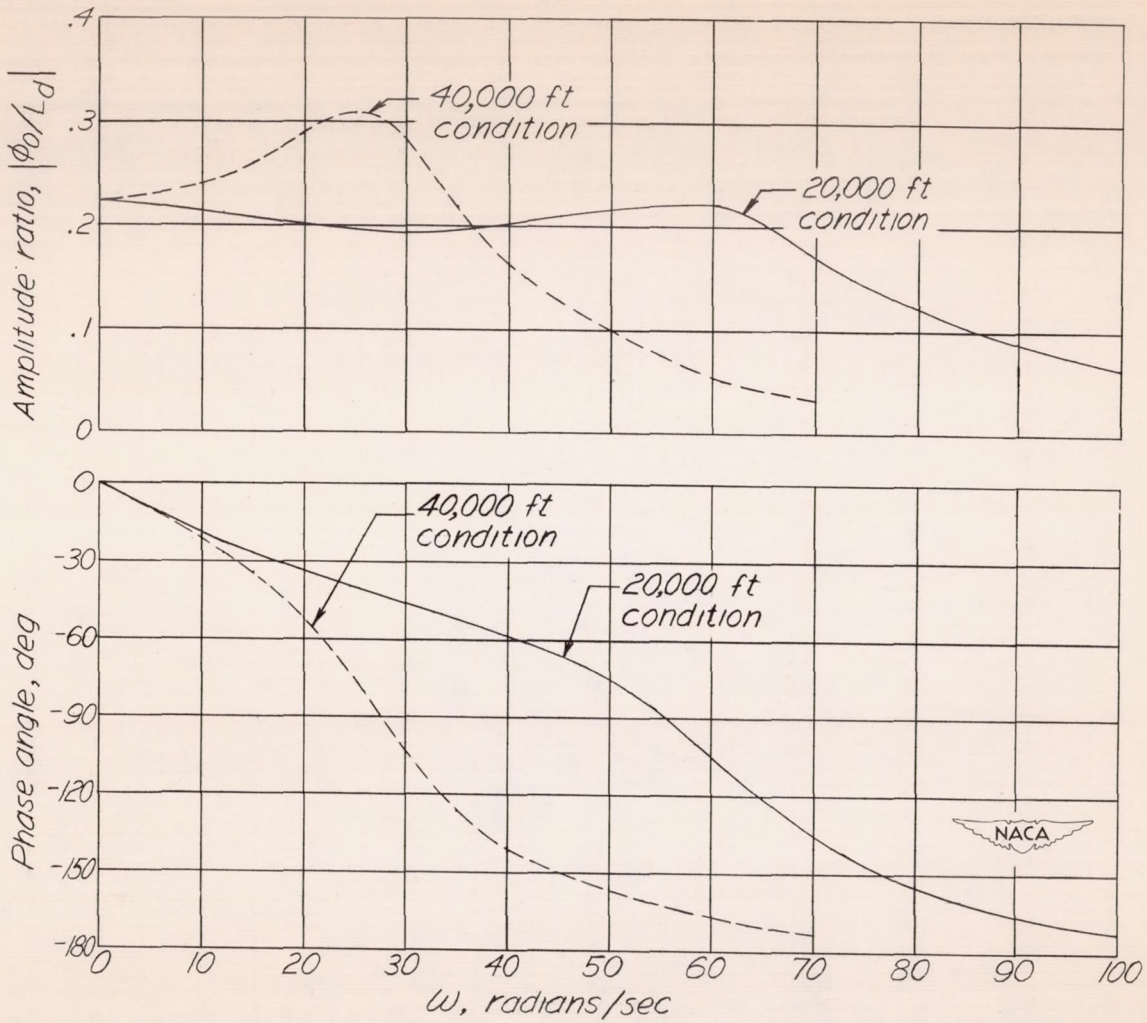

(b) Closed-loop system frequency responses, $\phi_o/L_d(j\omega)$.

Figure 14.- Concluded.

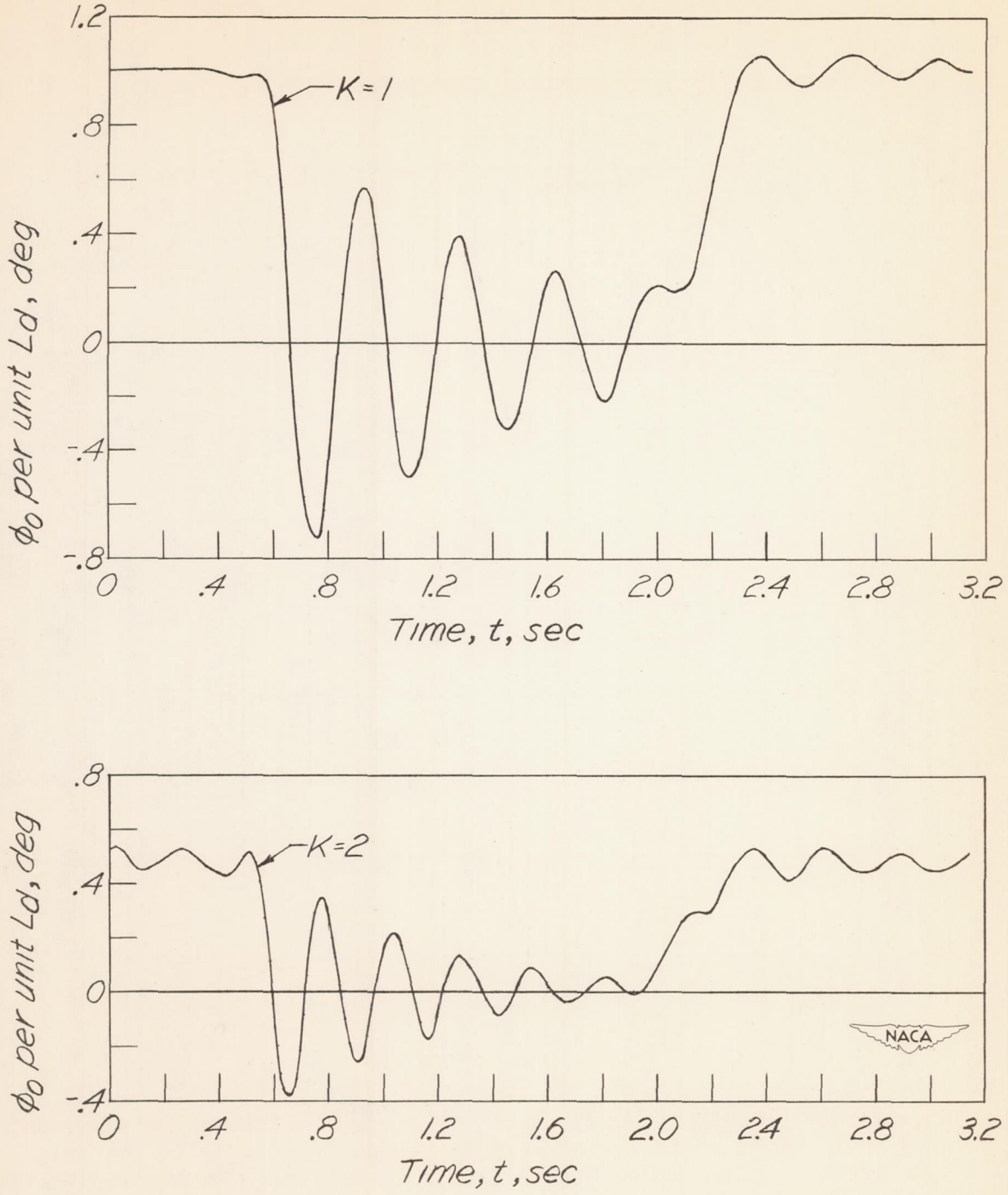

Figure 15.- Transient responses of ϕ_o to the ramp input of L_d for the airframe and gyro-actuated control system, for two values of control-gearing ratio K at the 20,000-foot (least oscillatory) flight condition. Input period, 3.14 seconds. Zero time arbitrarily chosen during the Fourier synthesizer cycle.

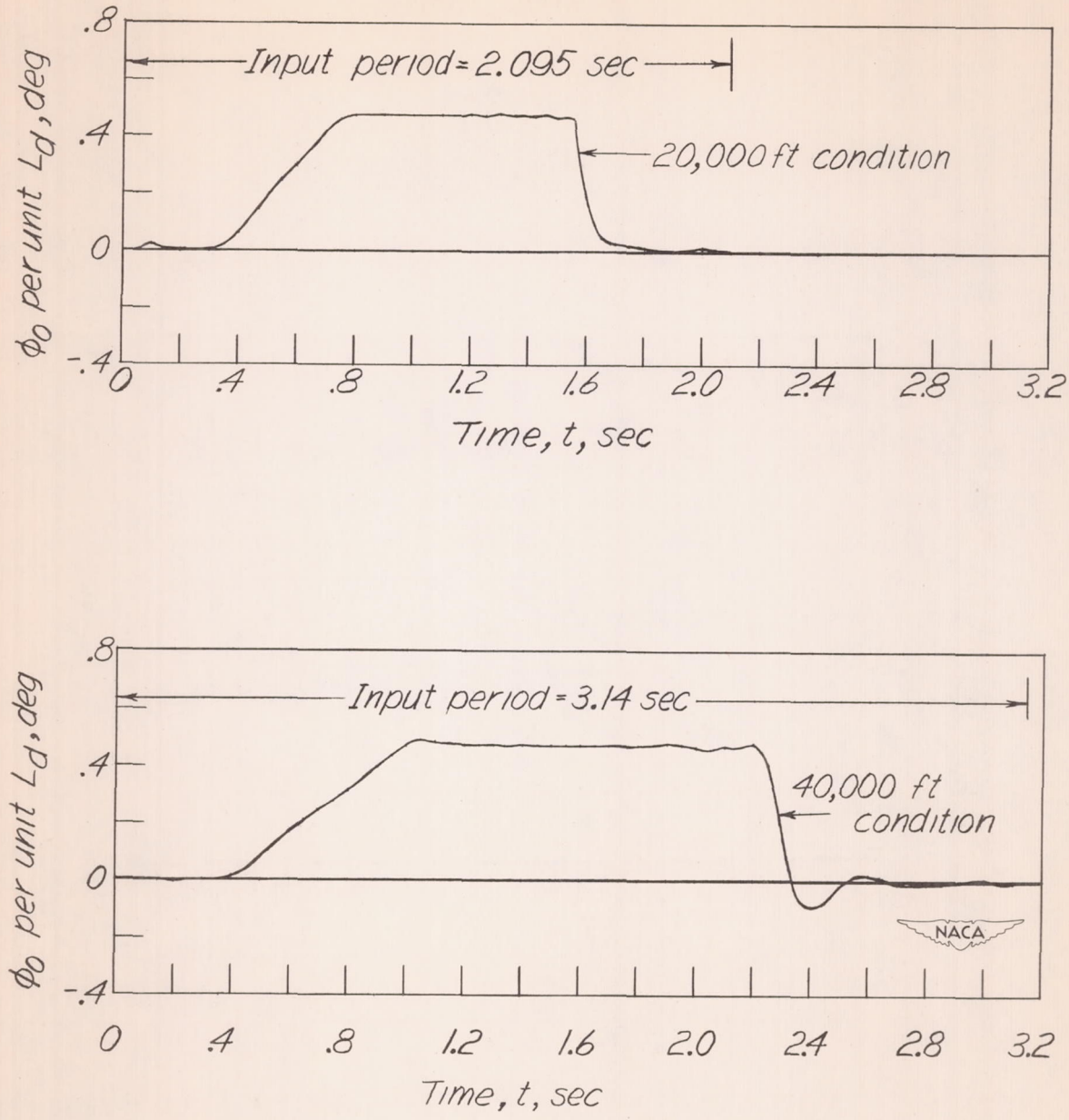

Figure 16.- Transient responses of the system including the airframe, gyro-actuated control, and rate gyro-pneumatic servo to the ramp input of L_d for the extreme flight conditions. Rate-servo static sensitivity, 0.1. Gyro-actuated-control K = 2.1. Zero time arbitrarily chosen during the Fourier synthesizer cycle.

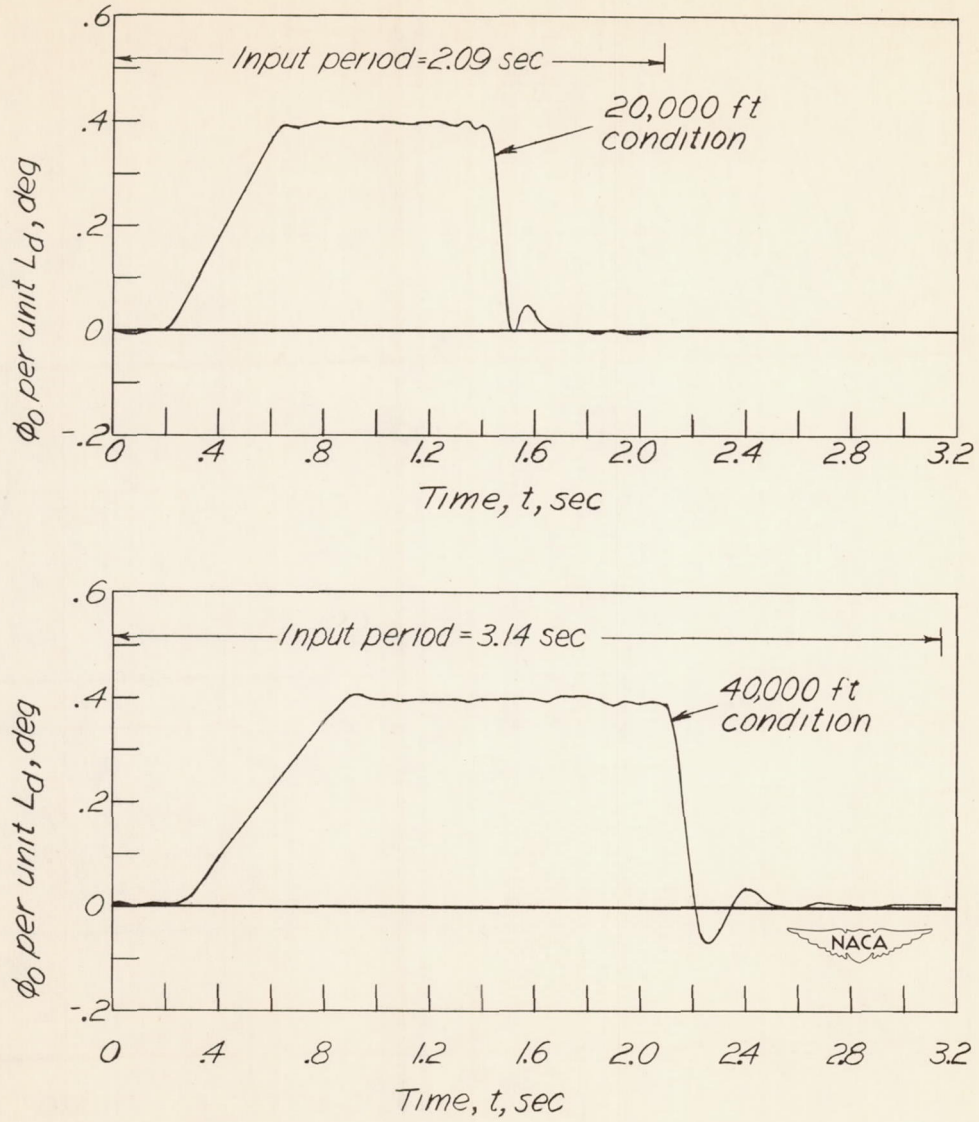

Figure 17.- Transient responses of the airframe and electronic-hydraulic autopilot with $\alpha = 3$, $\omega_1 = 15$ lead network to the ramp input of L_d for the extreme flight conditions. Gain adjusted 8 decibels. Zero time arbitrarily chosen during the Fourier synthesizer cycle.

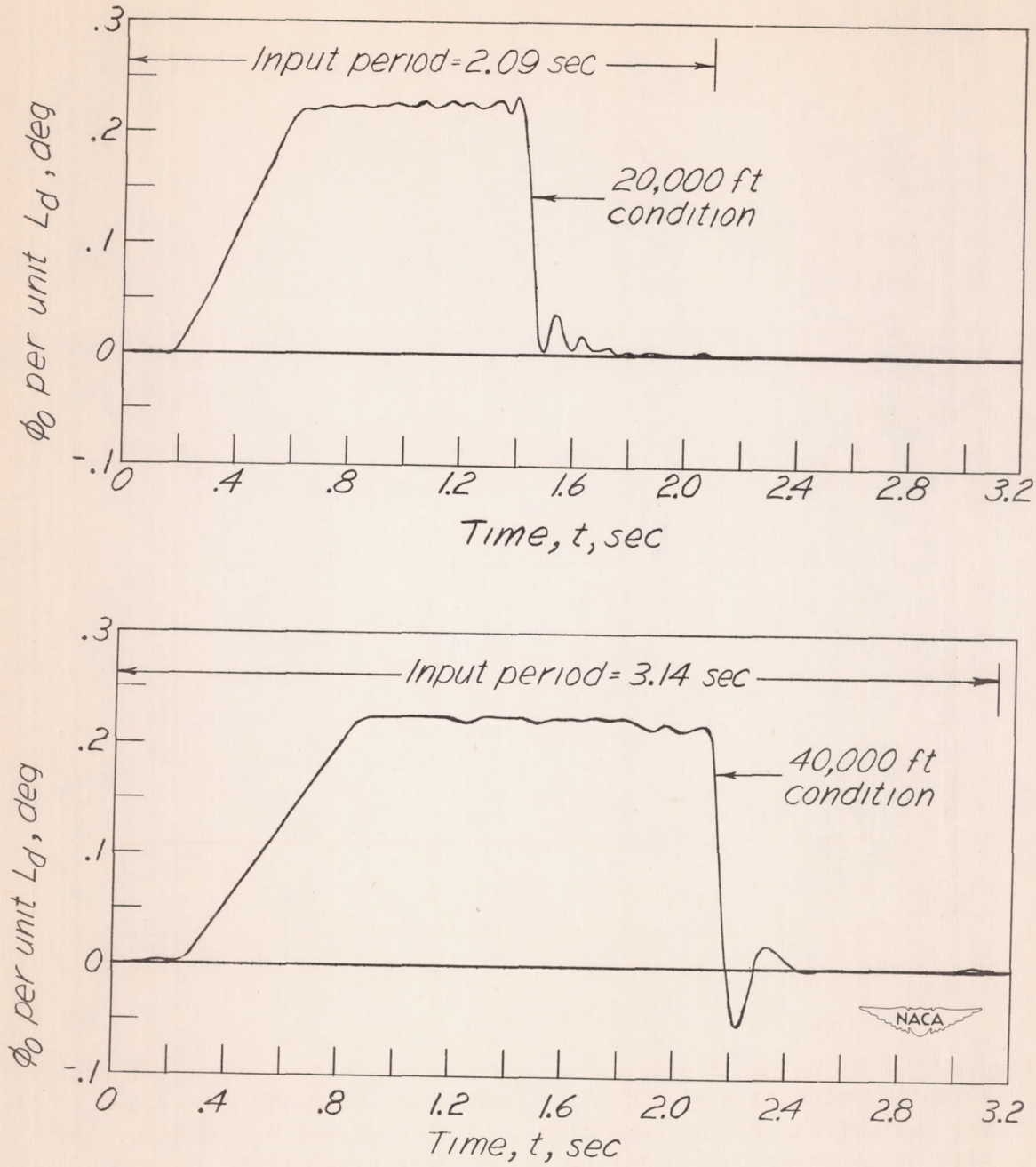

Figure 18.- Transient responses of the airframe and electronic-hydraulic autopilot with $\alpha = 3$, $\omega_1 = 20$ lead network, to the ramp input of L_d for the extreme flight conditions. Gain adjusted 13 decibels. Zero time arbitrarily chosen during the Fourier synthesizer cycle.